Molecular Therapy
Nucleic Acids
Original Article

Lentiviral gene therapy reverts GPIX expression and phenotype in Bernard-Soulier syndrome type C

Gonzalo Martinez-Navajas,[1,2] Jorge Ceron-Hernandez,[1,2] Iris Simon,[1,2] Pablo Lupiañez,[1,2] Sofia Diaz-McLynn,[1] Sonia Perales,[1,2,3] Ute Modlich,[4] Jose A. Guerrero,[5,6] Francisco Martin,[1,7] Teresa Sevivas,[8] Maria L. Lozano,[9] Jose Rivera,[9,10] Veronica Ramos-Mejia,[1] Claudia Tersteeg,[11] and Pedro J. Real[1,2,3]

[1]GENyO, Pfizer-Universidad de Granada-Junta de Andalucia Centre for Genomics and Oncological Research, PTS, Granada, Avenida de la Ilustracion 114, 18016 Granada, Spain; [2]University of Granada, Department of Biochemistry and Molecular Biology I, Faculty of Science, Avenida Fuentenueva S/n, 18071 Granada, Spain; [3]Instituto de Investigación Biosanitaria Ibs.GRANADA, Granada, Spain; [4]Department of Gene and Cell Therapy, Institute of Regenerative Medicine, University of Zürich, Wagistrasse 12, 8952 Schlieren-Zürich, Switzerland; [5]Department of Haematology, University of Cambridge, Cambridge, UK; [6]National Health Service Blood and Transplant, Cambridge Biomedical Campus, Cambridge, UK; [7]University of Granada, Department of Biochemistry and Molecular Biology III and Immunology, Faculty of Medicine, Avenida Ilustracion S/n, 18016 Granada, Spain; [8]Serviço de Sangue, Medicina Transfusional e Imunohemoterapia Do Centro Hospitalar e Universitário de Coimbra, Coimbra, Portugal; [9]Servicio de Hematología y Oncología Médica, Hospital Universitario Morales Meseguer, Centro Regional de Hemodonación, Universidad de Murcia, IMIB-Pascual Parrilla, CIBERER-ISCIII, U765 Murcia, Spain; [10]Grupo Español de Alteraciones Plaquetarias Congénitas (GEAPC), Madrid, Spain; [11]Laboratory for Thrombosis Research, IRF Life Sciences, KU Leuven Campus Kulak Kortrijk, Kortrijk, Belgium

Bernard-Soulier syndrome (BSS) is a rare congenital disease characterized by macrothrombocytopenia and frequent bleeding. It is caused by pathogenic variants in three genes (*GP1BA*, *GP1BB,* or *GP9*) that encode for the GPIbα, GPIbβ, and GPIX subunits of the GPIb-V-IX complex, the main platelet surface receptor for von Willebrand factor, being essential for platelet adhesion and aggregation. According to the affected gene, we distinguish BSS type A1 (*GP1BA*), type B (*GP1BB*), or type C (*GP9*). Pathogenic variants in these genes cause absent, incomplete, or dysfunctional GPIb-V-IX receptor and, consequently, a hemorrhagic phenotype. Using gene-editing tools, we generated knockout (KO) human cellular models that helped us to better understand GPIb-V-IX complex assembly. Furthermore, we developed novel lentiviral vectors capable of correcting GPIX expression, localization, and functionality in human *GP9*-KO megakaryoblastic cell lines. Generated *GP9*-KO induced pluripotent stem cells produced platelets that recapitulated the BSS phenotype: absence of GPIX on the membrane surface and large size. Importantly, gene therapy tools reverted both characteristics. Finally, hematopoietic stem cells from two unrelated BSS type C patients were transduced with the gene therapy vectors and differentiated to produce GPIX-expressing megakaryocytes and platelets with a reduced size. These results demonstrate the potential of lentiviral-based gene therapy to rescue BSS type C.

INTRODUCTION

Bernard-Soulier syndrome (BSS) is an extremely rare, autosomal recessive disease characterized by severe macrothrombocytopenia associated with frequent mucocutaneous bleeding.[1,2] Its prevalence is less than 1 in 1,000,000, although it may be underestimated.[3] Its clinical manifestations include, but are not limited to, purple, epistaxis, menorrhagia, gingival, and gastrointestinal bleeding.

Molecularly, the origin of the disease is caused by pathogenic variants of the *GP1BA*, *GP1BB,* or *GP9* genes that encode three components of the GPIb-V-IX glycoprotein complex, a membrane receptor for von Willebrand factor (vWF) expressed in megakaryocytes (MKs) and mature platelets.[4] According to the affected gene, we can differentiate BSS type A1 (*GP1BA*), BSS type B (*GP1BB*), or BSS type C (*GP9*). Most cases of BSS are caused by homozygous or compound heterozygous mutations. Some monoallelic variants affecting these genes cause an autosomal dominant form of macrothrombocytopenia, mostly asymptomatic.[5,6] To date, about 100 different variants have been reported in BSS patients worldwide spread across all three genes. The most commonly mutated gene is *GP9* (44% of cases), followed equally by *GP1BA* (28%) and *GP1BB* (28%).[5]

GPIb-V-IX complex is the receptor for vWF, a multimeric protein required for the initial adhesion and activation of platelets upon vascular injury, resulting in the formation of a platelet thrombus that arrests bleeding.[1,2] Genetic variants in *GP1BA*, *GP1BB,* or *GP9* genes can result in the absence or dysfunction of

Received 3 February 2023; accepted 8 June 2023;
https://doi.org/10.1016/j.omtn.2023.06.008.

Correspondence: Pedro J. Real, PhD, Gene Regulation, Stem Cells and Development Lab, GENyO, Pfizer-Universidad de Granada-Junta de Andalucia Centre for Genomics and Oncological Research, PTS Granada Avda. de la Ilustración 114, Granada 18016, Spain.
E-mail: pedro.real@genyo.es

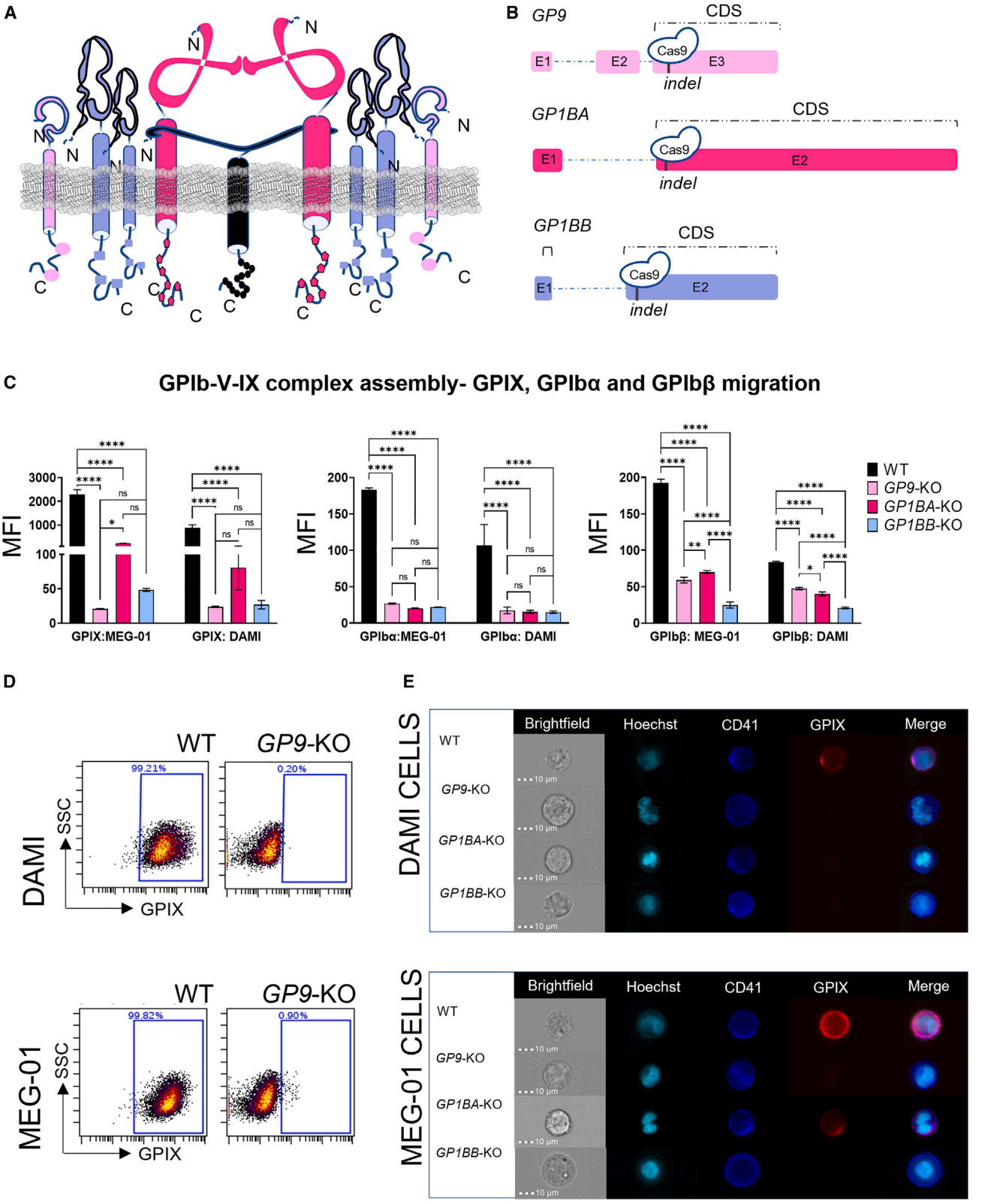

(legend on next page)

the GPIb-V-IX complex and consequently frequent bleeding.[7] Currently, the standard treatment for BSS is similar to that of other bleeding-associated genetic thrombopathies, including antifibrinolytic agents, desmopressin, or hormonal treatments in women.[8,9] In cases of trauma or major surgical interventions, platelet transfusion may be required. Patients receiving repeated platelet transfusions are at high risk of developing alloantibodies against molecules in the HLA or the proteins of the GPIb-V-IX complex, resulting in platelet refractoriness. Therefore, platelet transfusion should be restricted as much as possible and, when required, the use of leukoreduced platelets obtained from a single donor with a compatible HLA is recommended.[8]

Hematopoietic stem cell (HSC) transplantation from donors with identical HLA has been successfully tested in few BSS patients who had developed platelet refractoriness and had healthy family members who served as compatible donors.[10,11] However, autologous HSC transplantation of genetically rescued HSCs would be a safer option for BSS patients with no HLA-compatible donors. Being a monogenic disease, BSS is a future candidate for replacement gene therapy like other platelet disorders.[12]

In the last decades, gene therapy has been successfully used for the treatment of monogenic diseases,[13] including several inherited hematopoietic diseases such as X-associated severe combined immunodeficiency (SCID-X1),[14] Wiskott-Aldrich syndrome,[15,16] β-thalassemia,[14,17,18] and Fanconi Anemia Subtype A (FA-A).[19] Few genetic rescue studies have been conducted on BSS animal models *in vivo*. Ware et al. generated a *Gp1ba* knockout (KO) mouse model that recapitulated many of the characteristics of BSS patients and could be rescued by overexpression of the human *GP1BA* gene by transgenic technology.[20] Later, Kanaji et al. used a lentiviral vector-based gene therapy strategy to fully correct platelet defects in this murine model.[21] Similarly, Strassel et al. used lentiviral vectors to overexpress human *GP1BB* reverting GPIb-V-IX complex deficiency in *Gp1bb* KO mice.[22]

Significant advances in the optimization of megakaryocytic differentiation from human pluripotent cells have been achieved.[23–25] Recently, Mekchay et al. generated induced pluripotent stem cells (iPSCs) from BSS type A1 and type B patients.[26] Platelets derived from BSS-iPSCs were larger than their wild-type (WT) counterparts. Importantly, lentiviral correction restored GPIb-V-IX expression, improved platelet production, and reduced platelet size in both BSS-iPSC models.

Although *GP9* is the most commonly affected gene in BSS, no genetic rescue studies have been conducted in BSS type C disease models to date. Here, we report the generation and characterization of new human cellular models for BSS type C using CRISPR-Cas9 gene-editing technology. We demonstrate that lentiviral expression of human WT *GP9* restores GPIb-V-IX complex expression, localization and function in *GP9*-KO cells. Moreover, we show that this new gene therapy tool rescues GPIX expression in MKs and platelets derived from *GP9*-KO iPSCs cellular models and two independent BSS type C patients.

RESULTS

GP9, *GP1BA,* and *GP1BB* gene-editing KOs prevent GPIb-V-IX complex assembly

The GPIb-V-IX receptor is localized on the MKs and platelet surface membrane and is assembled by four subunits: GPIbα, GPIbβ, GPIX, and GPV, in 2:4:2:1 stoichiometry[27] (Figure 1A). To investigate the contribution of each subunit in the GPIb-V-IX assembly, we knocked out *GP9*, *GP1BA,* or *GP1BB* in two different megakaryoblast cell lines (DAMI and MEG-01) using CRISPR-Cas9. Single guide RNAs (sgRNAs) specific for *GP1BA*, *GP1BB,* and *GP9* genes were selected at the beginning of the coding sequence (CDS) considering maximal score and minimal off-target criteria (Figure 1B). These sgRNAs together with Cas9-expressing vector were lipofected into DAMI and MEG-01 WT cells, and single-cell clones were isolated for each cell model carrying different mutations. In all cases, open reading frames from both alleles were interrupted by frameshift variants leading to truncated proteins lacking their functional extracellular domains (Tables S1–S3).

Next, we analyzed CD42A (GPIX), CD42B (GPIbα), and CD42C (GPIbβ) expression by flow cytometry in all WT and KO cellular models. Every single component was expressed in both DAMI and MEG-01 WT cells. Interestingly, the expression level of all the proteins was higher in MEG-01 WT than in DAMI WT cells (Figures 1C and S1). As expected, GPIX expression was completely absent in both *GP9*-KO cell line models and variable in the other two KO models (Figures 1C–1E and S1). While GPIX expression was absent or residual in *GP1BB*-KO cells ($p < 0.0001$), its expression was significantly reduced for *GP1BA*-KO, in terms of mean fluorescence intensity (MFI) (∼230 vs. ∼2300) and percentage of positive cells (∼60%) in MEG-01 cells ($p < 0.0001$). Similarly, GPIX MFI (∼80 vs. ∼880) and percentage (∼30%) were reduced ($p < 0.0001$) in the DAMI *GP1BA*-KO cellular model. Importantly, GPIbα surface expression is absent in terms of percentage in all three KO models for

Figure 1. Modeling Bernard-Soulier syndrome in megakaryoblastic cell lines

(A) Schematic representation of the GPIb-V-IX receptor, indicating the composition and stoichiometry of the subunits. (B) KO establishment for each subunit of the GPIb-V-IX receptor with the CRISPR-Cas9 system: *GP1BA*, *GP1BB,* and *GP9* genes. (C) Mean fluorescence intensity (MFI) comparison of GPIX (left panel), GPIbα (middle panel), and GPIbβ (right panel) subunits for DAMI and MEG-01 WT and KO cell lines. (D) Flow cytometry dot plots indicating GPIX expression for WT and *GP9*-KO (BSS) in DAMI (top) and MEG-01 cells (bottom). (E) Representative ImageStream images of WT, *GP9*-KO, *GP1BA*-KO, and *GP1BB*-KO in both megakaryoblastic cell models, DAMI (top), and MEG-01 (bottom) cells. Channels indicate the localization and expression levels for Hoechst (nucleic DNA, cyan), CD41 (blue), and GPIX (red). The last channel corresponds to the merged channels, except for the brightfield. Data represent mean ± SD for three independent experiments. Statistical significance was assessed with ANOVA two-way plus Tukey multiple comparison test (ns = non-significant, *$p < 0.05$, **$p < 0.01$, and ****$p < 0.0001$).

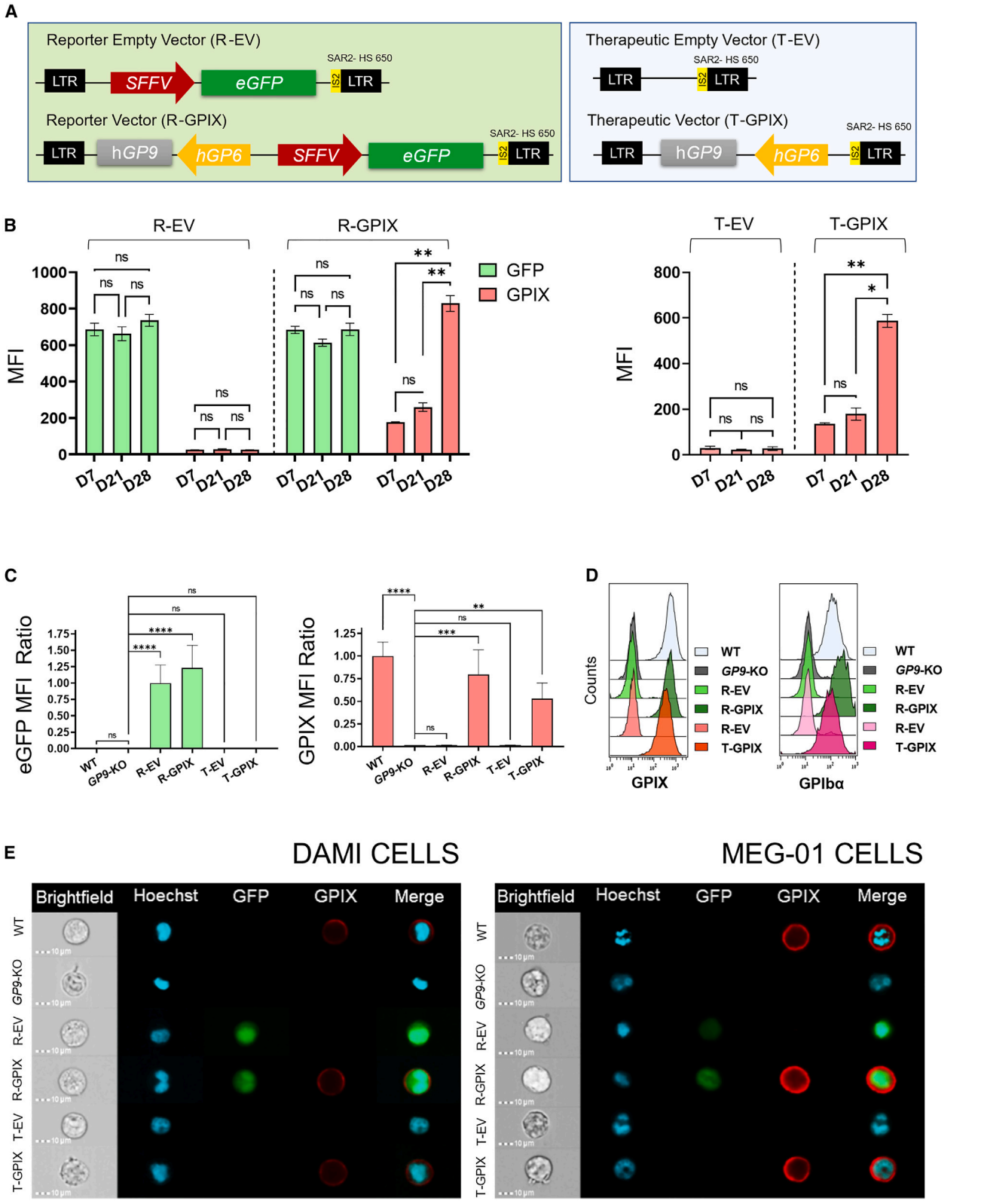

(legend on next page)

both cell lines ($p < 0.0001$) (Figures 1C and S1). In contrast, GPIbβ subunit could eventually be exported to the cell membrane in *GP9*-KO: ∼60 vs. ∼190 and 20% positive cells in MEG-01; and ∼50 vs. ∼85 and 10% positive cells in DAMI cell model. Likewise, GPIbβ expression was observed in MEG-01 *GP1BA*-KO cells (∼70 vs. ∼190 and 50% of positive cells), but it was less evident in DAMI *GP1BA*-KO cells (∼40 vs. ∼85 and only 5% of positive cells) (Figures 1C and S1).

ImageStream platform allowed us to determine protein expression and localization at the single-cell level. We analyzed GPIX expression in *GP9*-KO, *GP1BA*-KO, and *GP1BB*-KO cell models. In line with the flow cytometry results, MEG-01 WT cells expressed higher levels of GPIX on the cell surface than DAMI WT cells (Figure 1E). Regarding the KO models, GPIX expression is absent in all models, except for MEG-01 *GP1BA*-KO cells, where we could observe a markedly affected GPIX export to the cell surface in comparison with MEG-01 WT cells. In addition, CD41 was always expressed on the outer membrane, indicating that cells maintained their megakaryoblast commitment upon impaired GPIb-V-IX complex migration (Figure 1E).

Altogether, our results indicate that the lack of only one of the components of the GPIb-V-IX complex does not always impair the export of the remaining subunits to the cell surface. Focusing on BSS type C, both *GP9*-KO cell models lacked GPIX expression on the cell membrane, becoming ideal BSS type C cellular models for testing the efficacy of lentiviral vectors-based gene therapy tools.

GPIX lentiviral vectors rescue GPIX expression and localization in *GP9*-KO BSS cellular models

Lentiviral vectors (LVs) are one of the most successful tools to treat different hematopoietic malignancies.[28] We aimed to develop LVs overexpressing *GP9* to potentially treat BSS type C patients. To restrict GPIX expression to megakaryocytic lineage, we tested three MK-specific promoters previously described.[29] We selected a long version of the human *GP6* promoter (h*GP6L*(p)) because of its activity and specificity in human megakaryocytic cell models (Figure S2). Thus, we designed a therapeutic cassette composed of h*GP6L*(p) followed by the complete human *GP9* CDS. For the reporter construct (R-GPIX), we used the SEIs2Rev LV that contains an SFFV(p)-EGFP cassette, allowing us to check transduction efficiency.[23] For the therapeutic construct (T-GPIX), we removed the SFFV-EGFP cassette from the R-GPIX. Our LV backbones included an insulator sequence (SAR2-HS 650) that prevents epigenetic silencing after genomic integration.[30] As shown in Figure 2A, we used their empty vector counterparts, R-EV and T-EV, respectively, as negative controls.

First, we evaluated LV specificity in different human cell lines from the non-megakaryocytic lineage (Figure S3). 293-T (embryonic kidney cells), THP-1 (monocytic origin), and Jurkat (lymphocytic origin) cell lines were transduced with our four LV vectors and analyzed for EGFP and GPIX expression by flow cytometry. EGFP expression was detected in all three cell lines transduced with R-EV or R-GPIX vectors as expected due to constitutive SFFV(p)-EGFP regulation. Notably, none of the three cellular models tested showed any expression of GPIX on the cell membrane after transduction with either R-GPIX or T-GPIX.

Next, we used DAMI *GP9*-KO cells to test these four LVs (R-EV, R-GPIX, T-EV, and T-GPIX). The analysis of GPIX expression over 28 days for these LVs showed a relatively high and stable transduction of the reporter vectors, in terms of EGFP MFI (∼700) and percentage of EGFP-positive cells (∼80%) in both R-EV and R-GPIX, throughout the analysis (day 7 to day 28). As expected, only R-GPIX restored GPIX expression, observing an increase over time (MFI ∼800 and ∼75% of GPIX-positive cells on day 28) (Figure 2B, left and Figure S4A, left). Similarly, T-GPIX vector restored GPIX expression levels progressively during the time reaching the maximum MFI and percentage at day 28 (∼600 and ∼72% of GPIX-positive cells; $p < 0.01$), while T-EV vector could not recover GPIX expression (Figure 2B, right and Figure S4A, right).

We also evaluated the LVs in MEG-01 *GP9*-KO cells (Figures 2C and 2D). At day 28 of analysis, the transduction efficiency was very high, with ∼98% EGFP expression ($p < 0.0001$) for R-GPIX and R-EV constructs (Figure S4B, left panel), and similar MFI values showed by MFI ratio relative to R-EV (Figure 2C, left panel). Importantly, the GPIX expression, shown as MFI ratio in comparison with GPIX protein levels in MEG-01 WT cells, was very high (Figure 2C, right panel, and Figure 2D, left panel), and an excellent percentage of GPIX expression, around 98%, in both R-GPIX and T-GPIX vectors was also achieved (Figure S4B, right panel) ($p < 0.0001$) demonstrating their effectiveness. As expected, both R-EV and T-EV constructs did not recover GPIX expression (Figures 2C, 2D, and S4B).

Figure 2. Genetic rescue of *GP9*-KO megakaryoblastic cell models by GPIX lentiviral-mediated expression

(A) Schematic representation of lentiviral vector constructs: reporter empty vector (R-EV), reporter vector (R-GPIX), therapeutic empty vector (T-EV), and therapeutic vector (T-GPIX). (B) The evaluation of EGFP and GPIX mean fluorescence intensities (MFIs) over 28 days in DAMI *GP9*-KO cells transduced with reporter (left panel) or therapeutic vectors (right panel). (C) EGFP (left panel), GPIX (right top panel), and GPIbα (right bottom panel) MFI ratios at 28 days post-transduction. MFI ratios are relativized to WT expression for GPIX and GPIbα and to R-EV for EGFP. (D) Representative overlayed flow cytometry histograms for GPIX (top panel) and GPIbα (bottom panel) cell surface expression in WT, *GP9*-KO, and *GP9*-KO genetically rescued MEG-01 cells. (E) Representative single-cell images taken by ImageStream of WT, *GP9*-KO, and *GP9*-KO cells transduced with R-EV, R-GPIX, T-EV, and T-GPIX for DAMI (left panel) and MEG-01 (right panel). Channels indicate the localization and expression levels for Hoechst (nucleic DNA, cyan), EGFP (green), and GPIX (red). The last channel corresponds to the merged channels, except for the brightfield. Data represent mean ± SD for three independent experiments. Statistical significance was assessed with ANOVA two-way plus Tukey multiple comparison test (B) or ANOVA one-way plus Dunnett's multiple comparison test (C) (ns = non-significant, *$p < 0.05$, **$p < 0.01$, ***$p < 0.001$, and ****$p < 0.0001$).

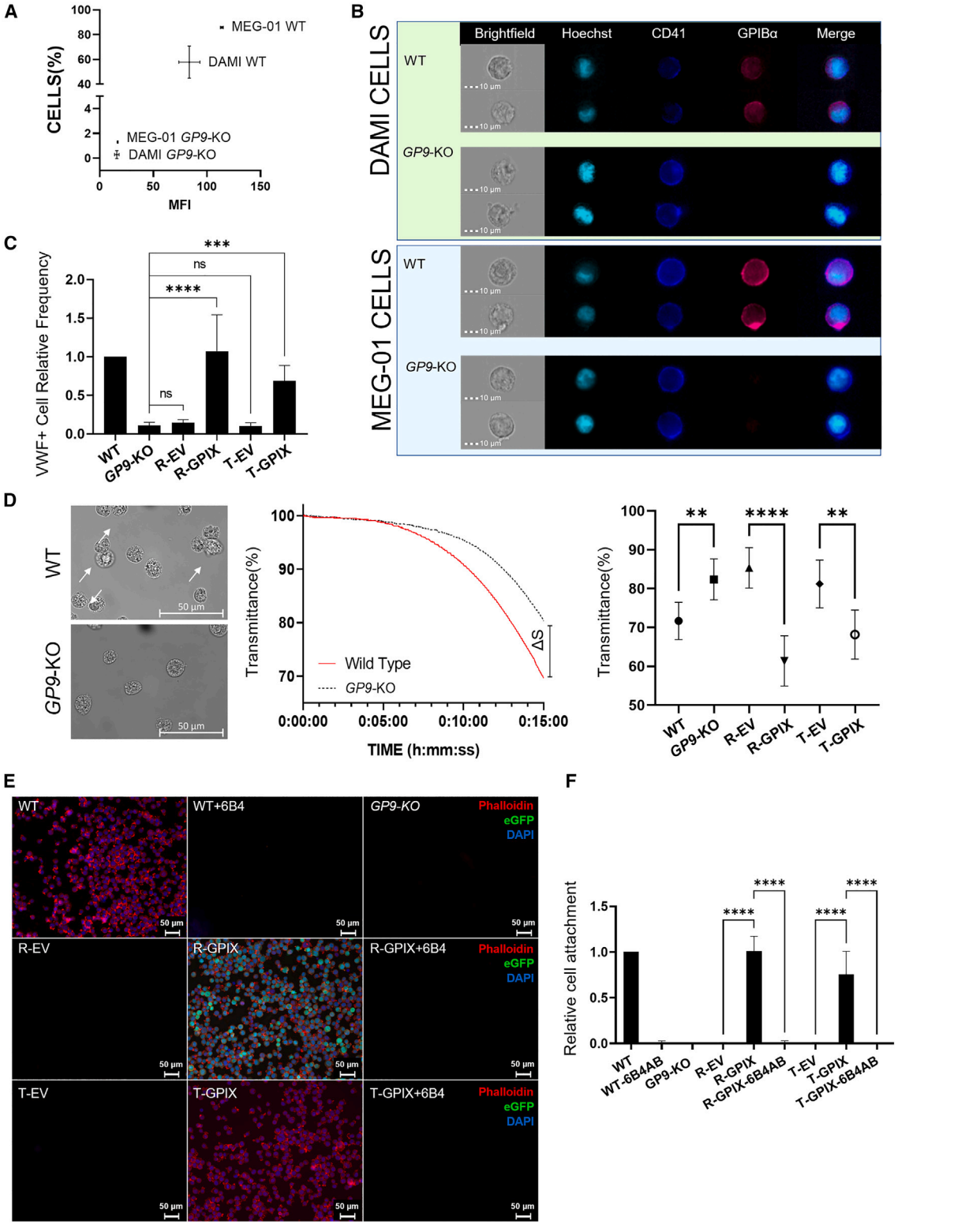

(legend on next page)

Furthermore, GPIX rescue with R-GPIX or T-GPIX LVs also restored GPIbα expression on the cell membrane with similar MFI values compared with WT cells (Figure 2D, right panel), showing GPIb-V-IX complex reassembly in the presence of exogenous GPIX.

Finally, we evaluated GPIX expression and localization in both *GP9*-KO cell models using ImageStream platform (Figure 2E). DAMI and MEG-01 *GP9*-KO cells transduced with R-EV and R-GPIX constructs showed a nuclear and cytosolic homogeneous expression of EGFP and only the cells transduced with R-GPIX restored GPIX expression localized on the plasma membrane. Similarly, DAMI and MEG-01 *GP9*-KO cells transduced with T-GPIX recovered the normal GPIX expression and distribution all on the cell surface.

Taken together, these results demonstrate that our LVs are specific for megakaryocytic cells and restore expression and localization of GPIX in both *GP9*-KO BSS cellular models.

Rescued *GP9*-KO BSS cellular models recover GPIb-V-IX receptor functionality *in vitro*

GPIb-V-IX complex binds to vWF through the interaction of the amino-terminal end of the GPIbα with the A1 domain of vWF.[31] Having demonstrated that our GPIX-expressing LVs restore both expression and localization of GPIX in *GP9*-KO cells, we aimed to verify that the rescued GPIb-V-IX complex was functional.

First, we analyzed GPIbα expression and localization in WT and *GP9*-KO cells by flow cytometry and ImageStream (Figures 3A and 3B). We compared MFI vs. cell percentage in DAMI and MEG-01 cellular models (Figure 3A). MEG-01 WT cells showed the highest MFI and percentage values by conventional flow cytometry and a clear distribution of GPIbα in the plasma membrane by ImageStream in comparison with DAMI WT cells (Figure 3B). Importantly, both *GP9*-KO BSS cellular models lost GPIbα expression on their cell surface. Therefore, we considered MEG-01 cellular models as the best system to test vWF binding capacity.

Next, we evaluated cellular binding capacity of cells to bind vWF upon stimulation with ristocetin by flow cytometry. As shown in Figure 3C, while MEG-01 WT cells bound vWF efficiently, we could not detect vWF binding to MEG-01 *GP9*-KO cells. Remarkably, MEG-01 *GP9*-KO cells transduced with LVs expressing GPIX (R-GPIX and T-GPIX) recovered their vWF binding capacity ($p < 0.0001$), reaching similar levels as MEG-01 WT cells. In contrast, MEG-01 *GP9*-KO cells transduced with their empty vector counterparts were not able to bind to vWF (Figure 3C). These results indicate that exogenous GPIX constitutes functional GPIb-V-IX complexes capable of interacting with vWF molecules *in vitro*.

Since ristocetin induces platelet agglutination in the presence of vWF via GPIbα,[32] we aimed to test whether megakaryocytic cells expressing GPIb-V-IX complex exposed to ristocetin and vWF could agglutinate by bridging GPIbα-vWF-GPIbα. However, due to the large size of the cells, the traditional RIPA assay does not work and therefore an adapted assay was developed. Here, cells were incubated with ristocetin and vWF for 2 min under stirring conditions, followed by sedimentation under static conditions. As shown in Figure 3D (left panel), MEG-01 WT cells formed doublets/multiplets in suspension, while MEG-01 *GP9*-KO cells were unable to aggregate with each other. Moreover, we could observe a clear difference in the sedimentation curve between MEG-01 WT and *GP9*-KO cells using a light-transmission aggregometer (Figure 3D, middle panel). MEG-01 WT cells sedimented faster due to the rapid formation of agglutinates, while MEG-01 *GP9*-KO cells showed higher transmittance percentage (less sedimentation rate) from minute 6 to the end of the analysis (15 min). Importantly, MEG-01 *GP9*-KO rescued with GPIX-expressing LVs (R-GPIX and T-GPIX) showed similar or even higher agglutination properties than MEG-01 WT cells. Endpoint data for each lentiviral transduction are shown in Figure 3D, right panel. Comparison of reporter vectors, R-EV vs. R-GPIX (80% vs. 60% transmittance, respectively), demonstrated a higher sedimentation rate after the genetic rescue. Similarly, MEG-01 *GP9*-KO transduced with the therapeutic vector (T-GPIX) achieved percentages of transmittance identical to MEG-01 WT cells.

To confirm GPIbα adhesion to surface-coated vWF, we performed vWF-coating assays in the presence of botrocetin (Figure 3E). This molecule has been isolated from *Bothrops jararaca* snake venom and, similarly to ristocetin, induces a conformational change in vWF that promotes platelet agglutination.[33] MEG-01 WT cells

Figure 3. Evaluation of vWF-GPIbα interaction in genetically rescued *GP9*-KO cells

(A) Comparison of the percentage of positive cells vs. mean fluorescence intensity (MFI) for GPIbα subunit expression in MEG-01 and DAMI WT and *GP9*-KO models. (B) Representative ImageStream images for DAMI and MEG-01 individual cells indicating Hoechst (cyan), CD41 (blue), and GPIbα (pink) expression levels. The last channel corresponds to the merger of the other channels, except for the brightfield. (C) Relative frequency of vWF^+ cells in WT, *GP9*-KO cells, and *GP9*-KO cells transduced with R-EV, R-GPIX, T-EV, and T-GPIX. Percentages were acquired by flow cytometry and relativized to WT percentage. (D) Example of a 100X image of WT and *GP9*-KO cells (right panel) previously incubated with a vWF-Ristocetin mixture over a 15-min period and their associated sedimentation curves showed as differential sedimentation rate (ΔS) (left panel). Endpoint data were transferred to the right panel, where we indicated the differences for each pair: WT vs. *GP9*-KO, R-EV vs. R-GPIX, and T-EV vs. T-GPIX. (E) Immunocytofluorescence of cells incubated with botrocetin on a vWF coating. Merged channels of phalloidin (red), DAPI (blue), and GFP (green) can be observed when cells adhere to vWF. The first row shows the vWF binding behavior of WT cells, WT cells incubated with 6B4, GPIbα-blocking antibody, and *GP9*-KO cells. The second and third rows illustrate cell behavior when *GP9*-KO cells were transduced with R-EV, R-GPIX, and R-GPIX+6B4 (second row) and T-EV, T-GPIX, and T-GPIX+6B4 (third row). (F) Data transferred to a graph. The bars represent the number of vWF-adherent cells relative to vWF-adherent WT cells. Data represent mean ± SD for three independent experiments. Statistical significance was assessed with ANOVA one-way plus Dunnett's multiple comparison test (C) or ANOVA one-way and Holm-Šídák's multiple comparison test (D and F) (ns = non-significant, $^{**}p < 0.01$, $^{***}p < 0.001$, and $^{****}p < 0.0001$).

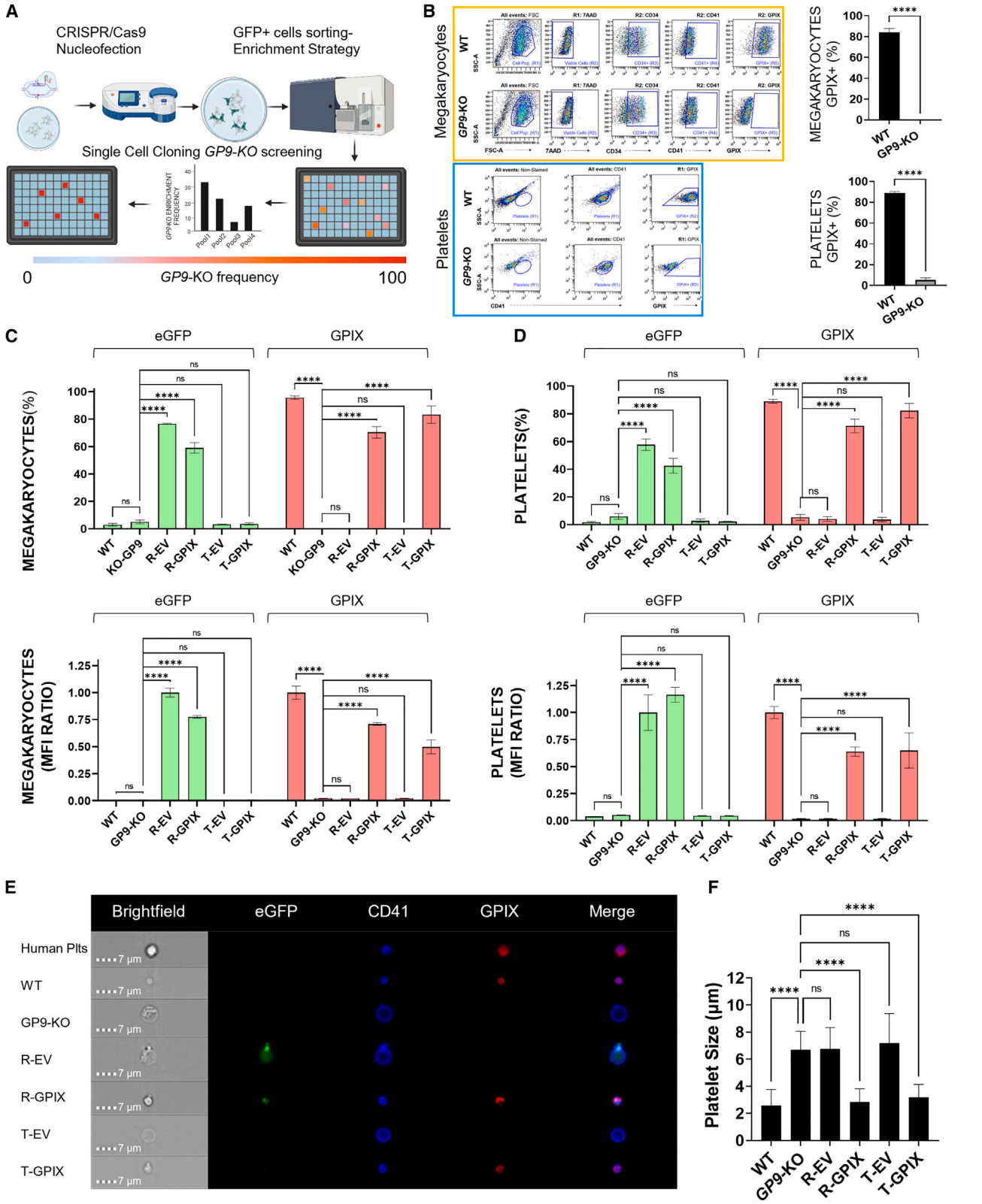

(legend on next page)

incubated with EDTA, to prevent an αIIbβ3 integrin adhesion to vWF, and botrocetin were able to attach to vWF-coated well surface (Figure 3E, top left panel). To demonstrate the specificity of this interaction, GPIbα-blocking antibody 6B4 was added.[34] In the presence of 6B4 blocking antibody, cells were unable to recognize and attach to vWF-coated surfaces, having the same behavior as MEG-01 *GP9*-KO cells lacking GPIbα (Figure 3E, top central and right panels). MEG-01 *GP9*-KO cells transduced with GPIX-expressing vectors (R-GPIX and T-GPIX) regained vWF binding capacity, while the specificity of the interaction was demonstrated with 6B4 blocking antibody (Figure 3E, middle central and right panels for R-GPIX; bottom central and right panels for T-GPIX). In contrast, MEG-01 *GP9*-KO cells transduced with empty vectors (R-EV and T-EV) failed to bind to coated vWF (Figure 3E, middle and bottom left panels). To quantitatively analyze cellular attachment to vWF-coated surfaces, we performed at least three independent replicates for every cellular model and experimental condition (Figure 3F).

Altogether, we have demonstrated that lentiviral transduction of *GP9*-KO cells with exogenous GPIX restored a functional GPIb-V-IX able to interact through its reassembled GPIbα subunit with soluble or immobilized vWF.

BSS-iPSC model reproduces the disease and can be corrected using GPIX-expressing lentivirus

To further demonstrate the efficacy of our GPIX-expressing LVs, we also evaluated these tools in iPSCs, which is the most appropriate physiological human BSS model available. During megakaryocytic differentiation, iPSCs progress to mature MKs ($CD41^+/CD42^+$) capable of releasing functional platelets (Figure S5A).[23–25] iPSC megakaryocytic differentiation was performed as previously described by Moreau et al. using lentiviral overexpression of three essential transcription factors: GATA1, FLI1, and TAL1.[25] The differentiation process can be monitored analyzing several differentiation markers (Figures S5B and S5C).

The iPSC *GP9*-KO cellular model was created using the CRISPR-Cas9 technology previously described. As shown in Figure 4A, CRISPR-Cas9-expressing vector together with sgRNAs for *GP9* were introduced into WT iPSCs by nucleofection. Forty-eight hours later, $EGFP^+$ iPSCs were sorted and cultured in pools of few cell numbers (∼100 cells/pool). Since iPSCs do not express GPIX at the pluripotent stage, genomic DNA from different nucleofected cell pools were sequenced to analyze *GP9 locus*. From the most enriched pool, single-cell cloning was performed and several *GP9*-KO iPSC clones were isolated. Once characterized (Table S3), *GP9*-KO iPSCs were differentiated into MKs and platelets and analyzed by flow cytometry, demonstrating the lack of GPIX after 21 and 36 days for MKs and platelets, respectively (Figure 4B, left panels). $CD41^+/GPIX^+$ populations were ∼85% for WT and totally absent for *GP9*-KO iPSC derivatives (Figure 4B, right panels).

Next, BSS-iPSCs cells were transduced with EGFP reporter (R-EV and R-GPIX) or therapeutic vectors (T-EV and T-GPIX) and differentiated into MKs (Figure 4C) and platelets (Figure 4D). R-EV- and R-GPIX-transduced iPSCs generated MKs containing similar EGFP expression (∼70% and ∼60%, respectively, Figure 4C, upper panel). However, platelets generated from these MKs showed lower EGFP expression levels (∼60% and ∼40%, respectively) (Figure 4D, upper panel). Importantly, both R-GPIX and T-GPIX LVs restored GPIX expression in both MKs and platelets in terms of percentage (∼70% and ∼80%, respectively, Figures 4C and 4D, upper panels) and MFI ratio compared with WT iPSC derivatives (∼0.7 in both MKs and platelets, Figures 4C and 4D, lower panels) ($p < 0.0001$). The dynamics of megakaryocytic differentiation in GPIX-expressing *GP9*-KO iPSCs was similar to WT iPSCs with GPIX expression appearing from day 15 onward (data not shown).

Using ImageStream, we observed that platelets produced *in vitro* from WT iPSCs and human platelets from healthy donors co-express CD41 and GPIX on their cell surface (Figure 4E). Interestingly, *GP9*-KO-iPSC-derived platelets reproduced both the GPIX absence and the larger size in comparison with WT counterparts. *GP9*-KO-iPSCs transduced with reporter vectors generated EGFP-positive platelets. R-EV maintains a larger size and the absence of GPIX expression like non-transduced platelets from *GP9*-KO iPSCs. Finally, using ImageStream analysis tools, we determined the size of the platelets generated from the different iPSC cellular models (Figure 4F). The diameter of platelets derived from WT iPSCs was approximately 2.5 μm, whereas the platelets obtained from *GP9*-KO iPSCs doubled their size. Remarkably, platelets derived from GPIX-transduced *GP9*-KO iPSCs showed GPIX expression and reduced their size to their WT counterparts, thus reverting the BSS phenotype.

In summary, we have generated and characterized a novel iPSC model of BSS by gene editing using CRISPR-Cas9. Furthermore, we have demonstrated that GPIX-expressing LVs are very effective in restoring GPIX expression and the size of iPSC-derived platelets.

Figure 4. BSS type C model generation in iPSCs and its correction by GPIX lentiviral vector transduction on MKs and platelets

(A) Schematic diagram of *GP9*-KO creation and isolation process in iPSCs. (B) Left panel: Flow cytometry dot plots for WT and *GP9*-KO differentiated cells (day 21) and platelets (day 36) indicating differentiation surface markers. Right panel: Graphical data corresponding to $CD41^+/GPIX^+$ double-positive population in WT and *GP9*-KO MKs (top) or platelets (bottom). (C) Percentage (top panel) and MFI values (bottom panel) of MKs ($CD41^+$) on day 21 expressing EGFP or GPIX for WT, *GP9*-KO, or *GP9*-KO cells transduced with LVs. (D) Percentage (top panel) and MFI values (bottom panel) for CD41 expression in iPSC-derived platelets on day 36. (E) Representative ImageStream images of human platelets and platelets generated from all our iPSC models showing their size, cytosolic EGFP expression (green), CD41 (blue), and GPIX (red) surface expression in each case. (F) Representation of platelet diameter (μm) from WT, *GP9*-KO, and *GP9*-KO transduced iPSCs. Data represent mean ± SD for at least three independent experiments. Statistical significance was assessed with unpaired Student's t test (B), ANOVA two-way plus Dunnett's multiple comparison test (C and D), or ANOVA one-way plus Dunnett's multiple comparison test (F) (ns = non-significant, ****$p < 0.0001$).

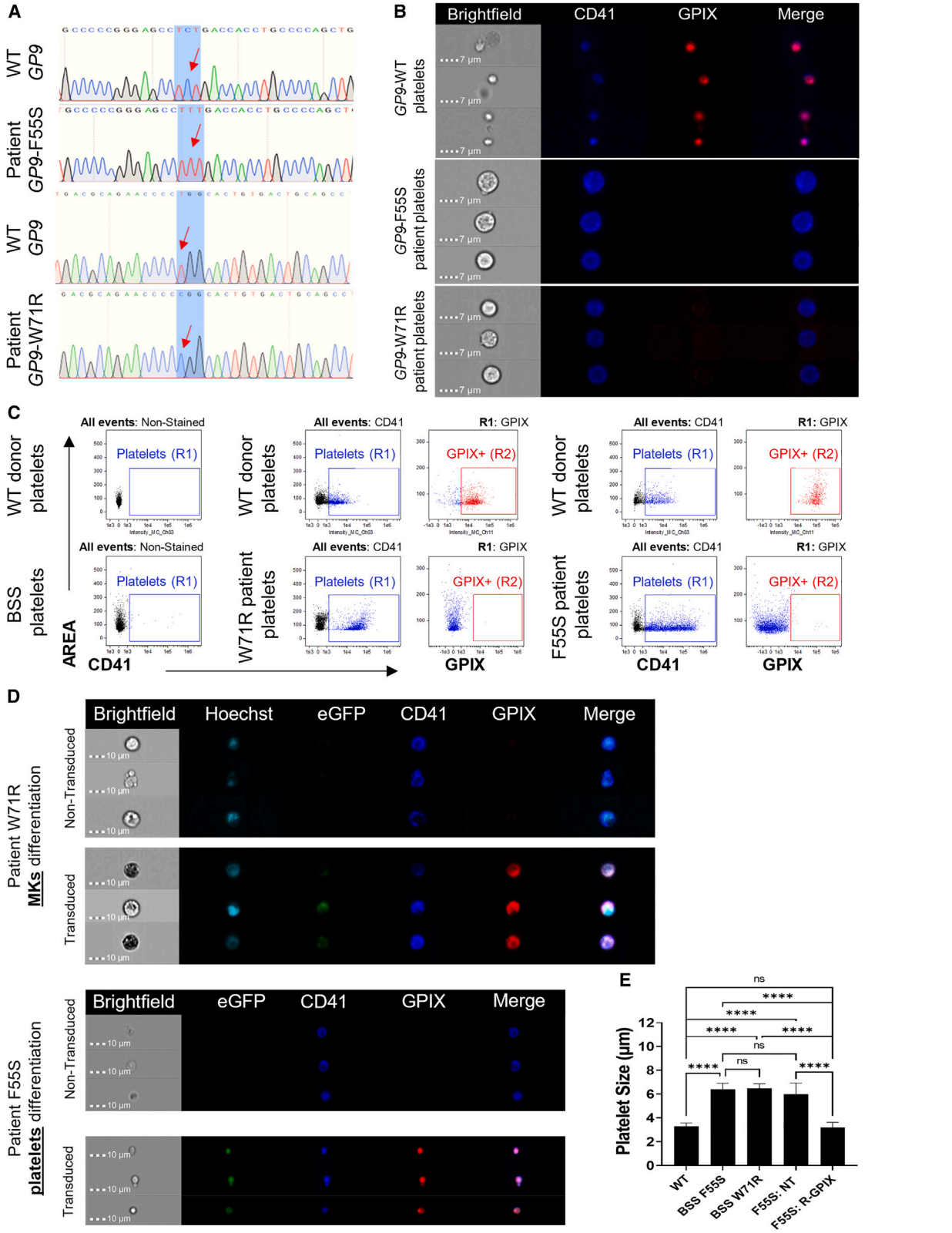

(legend on next page)

Rescue of GPIb-V-IX surface expression in MKs and platelets generated from HSCs of BSS patients

Our final aim was to genetically engineer HSCs from BSS type C patients, our future target cells for *ex vivo* therapy. Peripheral mononuclear blood cells were obtained from two unrelated BSS type C patients recruited in the multicentric Spanish project of inherited platelet disorders.[35] Genomic DNA was purified and sequenced to confirm the presence of homozygous variants p.Phe55Ser and p.Trp71Arg (Figure 5A). Patients' platelets were analyzed by ImageStream confirming GPIX absence, increased CD41 expression,[36] and large size compared with WT platelets (Figures 5B and 5C).

Due to the reduced number of circulating $CD34^+$ cells purified (~50,000 cells/50 mL blood), we only used the R-GPIX lentiviral vector, as this one allowed us to follow transduction efficiency and GPIX recovery by ImageStream. $CD34^+$ isolated HSCs from both patients were expanded, transduced with R-GPIX, and differentiated to MKs/platelets for 10 days. Non-transduced MKs neither expressed EGFP nor GPIX, while transduced cells re-established GPIX expression/localization together with EGFP cytoplasmatic expression (Figure 5D, upper panel). For platelet analysis, mature MK culture supernatants were collected, platelets were enriched by centrifugation, labeled with CD41 and GPIX, and analyzed by ImageStream. As shown in Figure 5D, platelets derived from non-rescued HSCs were larger and did not have GPIb-V-IX complex at surface, whereas platelets produced from transduced HSCs showed smaller size, expressed GPIX on the surface, and expressed EGFP. Finally, platelet size study using ImageStream analytical tools from WT donors, BSS patients, and CD34-derived platelets confirmed that R-GPIX LV not only restored GPIX expression but also, and more importantly, platelet size (Figure 5E). These results demonstrate that lentiviral-mediated therapy restores GPIX expression in MKs and platelets generated from primary HSCs isolated from BSS type C patients.

DISCUSSION

The assembly of the GPIb-V-IX receptor present in the plasma membrane of MKs and platelets occurs through the combination of four subunits: GPIbα, GPIbβ, GPIX, and GPV. These subunits interact in the endoplasmic reticulum and reach their mature forms inside the Golgi apparatus before being transported to the cell surface. Overexpression experiments performed in mammalian cells, L cells, and CHO cells demonstrated that GPIbα export to the plasma membrane is primarily dependent on GPIbβ and GPIX expression.[37] In contrast, GPV appears to play a secondary role in this process. Subsequently, CHO cells have gained popularity in the biotechnology industry due to their ability to produce very efficiently human cellular proteins containing posttranslational modifications, such as glycosylations.[38] As a result, they have emerged as the primary platform for analyzing GPIb-V-IX receptor assembly and the effects of diverse mutations identified in BSS patients.[39–45]

Despite its widespread use, the CHO cell model has its limitations, such as its non-human origin and it requires overexpression of the subunits, which may impact the physiological relevance of the results. To address this concern, researchers have conducted assays using human 293T cells.[43] Again, these cells do not naturally express the components of the GPIb-V-IX complex due to their origin. In light of these limitations, we evaluated the functionality of DAMI and MEG-01, two megakaryoblastic leukemia cell models that endogenously express and regulate the expression of all four subunits of the GPIb-V-IX complex. BSS cellular models were generated by introducing frameshift mutations with CRISPR-Cas9 at the beginning of *GP1BA*, *GP1BB,* and *GP9* coding sequences.

Interestingly, we found that GPIbα expression is most dependent on the presence of other subunits, as it is undetectable in both *GP1BB*-KO or *GP9*-KO cellular models. In line with our data, Dong et al. demonstrated that the surface expression of GPIbα is dependent on the co-expression of GPIbβ and GPIX proteins.[37] The absence of either of these subunits results in the targeting and degradation of GPIbα in the lysosomes. In a BSS type C patient carrying the p.Phe55Ser variant, Noris et al. confirmed reduced GPIbα expression using three different antibodies.[36] The percentage of GPIbα-positive platelets ranged from 41.5% to 86.6%. Subsequently, several studies have described reduced GPIbα expression, less than 10% relative expression, in all BSS patients analyzed, regardless of the disease-causing variant.[3,46,47] Furthermore, GPIX and GPIbα were absent in MKs and platelets from a BSS type C patient carrying a homozygous deletion of the entire *GP9* gene.[48] In contrast, BSS patients carrying the W127X pathogenic variant in *GP9,* originally described in Japan,[49] exhibit a deficiency of GPIX expression while displaying residual surface expression of GPIbα.[50] Subsequently, Takata et al. quantified GPIbα relative MFI expression compared with healthy controls, revealing that it ranged from 7% to 11% in this group of BSS patients.[45] Despite the reduced expression level of GPIbα, platelets from W127X patients were capable of binding to immobilized vWF under high-shear conditions *in vitro*.

Figure 5. BSS type C patients' characterization and generation of MKs-platelets from transduced and non-transduced BSS-HSCs

(A) Characterization of *GP9*-associated variants for two unrelated BSS patients. (B) Representative ImageStream platelet images from donor and BSS patients indicating size and expression of CD41 (blue) and GPIX (red) surface markers. (C) ImageStream dot plots obtained from BSS and donor platelets showing CD41 expression profile and GPIX-expressing platelets from this first population. (D) ImageStream events corresponding to differentiated MKs and platelets obtained from transduced and non-transduced W71R-BSS-HSCs and F55S-BSS-HSCs, respectively. The top panel shows MKs from the W71R patient and bottom panel shows platelets from F55S. Channels indicate the localization and expression levels for Hoechst (nucleic DNA, cyan), EGFP (green), CD41 (blue), and GPIX (red). The last channel corresponds to the merged channels, except for the brightfield. (E) Representation of platelet size showed by their diameter (μm) belonging to platelets from a human healthy control, W71R and F55S both BSS patients, and those produced from non-transduced and R-GPIX-transduced F55S isolated and differentiated $CD34^+$ cells. Data represent mean ± SD from $n \geq 11$ events. Statistical significance was assessed with ANOVA one-way plus Tukey multiple comparison test (ns = non-significant, ****$p < 0.0001$).

According to our results, GPIbβ is relevant for the assembly of the entire complex. In its absence, the remaining three subunits are not detectable at the plasma membrane, with the exception of a basal GPIX expression in MEG-01 *GP1BB*-KO cells. In contrast, the lack of GPIX or GPIbα subunits allows some expression of GPIbβ on the cell surface. In agreement, the GPIb-V-IX complex is fully absent in BSS type B patients,[6,51,52] and in a patient with velocardial syndrome with a hemizygous microdeletion of 22q11.2 containing the *GP1BB locus* and p.Pro96Ser variant in the other *GP1BB* allele.[53]

Our data also indicate that GPIbβ collaborates in GPIX export to the outer membrane, as can be observed for *GP1BA*-KO cells. This observation is supported by the absence of GPIX and GP1bα on the platelets of two siblings carrying a compound heterozygous frameshift (c.1601_1602delAT) and nonsense (c.1036C>T) variant in *GP1BA* that abrogated the production of GP1bα.[54] Similarly, GPIX expression could be observed in some BSS type A1 patients containing homozygous or compound heterozygous variants in *GP1BA*.[55,56] Additionally, overexpression experiments in CHO cells show that co-transfection of mutant *GP1BA*, with WT-*GP1BB* and WT-*GP9,* leads to a decreased GPIX expression in comparison with CHO cells expressing WT-*GP1BA*. In contrast, when WT-*GP1BA*, WT-*GP9,* and variant p.Asn64Thr *GP1BB* were co-transfected, none of the subunits could be detected,[52] suggesting GPIbβ-GPIX co-migration.[52,53,57]

Our results indicate that our new human KO cellular models are more suitable than CHO cells for investigating the BSS disease due to their ability to maintain a physiological allelic contribution. This allows us to observe GPIb-V-IX complex localization, complete agglutination experiments, or perform vWF-coating assays in the presence of ristocetin or botrocetin. Therefore, they will be more physiologically relevant than CHO cells. Using lentiviral transduction or CRISPR-Cas9 technology, we could study biallelic, monoallelic, or heterozygous dominant BSS-specific variants. In addition to vWF, the GPIb-V-IX complex can bind multiple molecules and cell receptors, and hence its role goes beyond platelet adhesion. Our new models would allow us to introduce variants causative of dominant BSS, other platelet disorders such as platelet-type von Willebrand disease, and even to study the relevance of this complex in the binding of other ligands/receptors as previously carried out in mice.[20,58] A similar strategy could be used to target other platelet receptors and disorders, e.g., ITGB3/ITGA2 in Glanzmann thrombastenia.[59]

Few previous studies have demonstrated that the use of LVs can recover GPIb-V-IX expression in BSS type A1 and B animal models.[21,22] We have designed LVs that are suitable for treating BSS type C patients resulting from any *GP9* nonsense or missense variant. Our LVs were functional recovering with high efficacy the stable expression and appropriate surface membrane localization of GPIX in three different *GP9*-KO cellular models: DAMI, MEG-01, and iPSCs. The percentage of rescued MKs and platelets in our *GP9*-KO iPSC cell model was very high (70%–80%) in comparison with previous studies. Thus, Mekchay et al. reprogrammed peripheral blood mononuclear cells from BSS type A1 and type B patients (*GP1BA*-iPSCs and *GP1BB*-iPSCs). Using pTREG-LVs to express WT *GP1BA* or *GP1BB,* their corresponding protein expression recovery was only 18% and 42%, respectively.[60]

We also evaluated the functionality of the GPIb-V-IX recovered by our LV therapy in *GP9*-KO cell models *in vitro*. vWF circulates through the bloodstream in a folded conformation. Once an injury occurs, subendothelial collagen becomes exposed binding vWF. In blood vessels, the high shear rates promote vWF unfolding, where the A1 domain becomes exposed being accessible to interact with the platelet GPIb-V-IX receptor via GPIbα. Therefore, platelets can firmly attach to vWF and initiate aggregation and subsequent coagulation.[61,62] In the absence of shear, ristocetin and botrocetin modify vWF, making the A1 domain accessible for GPIbα binding.[6,63] It is noteworthy that we could demonstrate that the functional capacity of MEG-01 WT stimulated with ristocetin to form cell agglutinates leading to sedimentation is lost in *GP9*-KO MEG-01 and recovered after transduction with GPIX-expressing vectors. Furthermore, this functionality was corroborated in cells plated over a vWF-coated surface and stimulated with botrocetin. Moreover, the specificity of the vWF-GPIbα interaction in these assays was confirmed with a GPIbα blocking antibody that abolished cellular adhesion.

The biological functionality of the rescued GPIb-V-IX was also observed in an iPSC cellular model. Platelets derived from *GP9*-KO iPSCs mimicked the BSS phenotype increasing their size in comparison with WT counterparts. Importantly, using ImageStream we could observe that platelets generated from rescued *GP9*-KO iPSCs recovered GPIX localization and reduced platelet size, in line with results in rescued *GP1BA*-iPSCs and *GP1BB*-iPSCs.[60] Together, these results showed that lentiviral therapy with GPIX-expressing vectors was not only able to restore the expression and localization, but also recovered full receptor assembly and functionality *in vitro*.

Finally, we evaluated the effectiveness of our novel gene therapy tools in HSC from two unrelated BSS type C patients previously diagnosed with the Spanish multicentric project on inherited platelets disorders.[35] Ethical concerns discourage aggressive procedures to obtain HSCs from bone marrow from these patients, but some HSCs are present and could be isolated from non-mobilized peripheral blood.[64–66] Purified HSCs were exposed to R-GPIX to track lentiviral transduction. Despite the reduced number of starting HSCs, we could recover CD41-GPIX expression in $EGFP^+$ MKs and platelets. As expected, non-transduced HSCs generated MKs and platelets lacking GPIX on their cell membrane. Furthermore, those platelets exhibited an increased size mimicking the macrothrombocytopenia described in BSS patients. In contrast, transduced HSCs produced smaller $GPIX^+/EGFP^+$ platelets, which reverted both phenotypes. The average size for WT, BSS, and BSS-rescued platelets produced *in vitro* is similar to that described previously.[3,43] These data in primary HSCs from BSS type C patients carrying different missense variants encourage further development of this novel gene therapy strategy for potential clinical use.

In conclusion, we have generated LVs that efficiently recover a functional GPIb-V-IX receptor in different *GP9*-KO cellular models and primary HSCs from BSS type C patients. Our results demonstrate that these novel LV-based therapies could be a therapeutic option for all BSS type C patients, regardless the *GP9* variant causing the disease. To the best of our knowledge, this is the first time that HSCs from BSS patients have been rescued *ex vivo*. Additional preclinical studies in animal models of BSS type C may be required to test the specificity, effectiveness, and biosafety of these gene therapy tools *in vivo*.

MATERIAL AND METHODS

Cell cultures

The MEG-01 cell line was acquired from ATCC. DAMI cells were a gift from Dr. Gutierrez, (University of Oviedo, Spain). Both megakaryoblastic cell lines were cultured in RPMI 1640 medium (Biowest) supplemented with 10% fetal bovine serum (FBS) (Biowest) and 1X penicillin/streptomycin (Sigma-Aldrich). Cells were passaged twice a week, seeding 1×10^5 cells/mL. THP-1 and Jurkat cells were grown under similar conditions. 293T cells were cultured in DMEM-high glucose media (Biowest) supplemented with 10% FBS and 1X penicillin/streptomycin. Twice a week cells were passaged (1:5–1:8) using 0.75X TrypLE Express (Gibco) for 5 min.

iPSC#1 line was obtained from Cambridge Biomedical Research Center Core Facility. This iPSC line was derived from adult dermal fibroblasts using integrative murine retroviral vectors and has been previously reported by Moreau et al. to efficiently produce MKs and platelets *in vitro*.[25] iPSCs were cultured over Matrigel-coated (BD Biosciences) T25 flasks in Essential 8 Medium (E8).[67] Confluent cultures were split (1:5–1:8) using PBS-EDTA (0.5 mM) for 5–8 min. The first day after passage, cells were supplemented with 10 μM Y-27632 2HCl (Deltaclon).

All cell lines used in this study were grown at 37°C and 5% CO_2 in a humid incubator.

Flow cytometry analysis

Cells were collected and washed once with PBS. After centrifugation ($150 \times g$, 5 min), cells were resuspended to a final concentration of 1×10^6 cells/mL in PBS; 100 mL of cells was then supplemented with antibody cocktails according to the experiment (1:100 of each antibody): anti-human CD42a-APC (Miltenyi Biotech), CD42b-APC (Miltenyi Biotech), rat anti-human RAM.1[68] (CD42C) conjugated with goat anti-rat Alexa Fluor 488 (Invitrogen), anti-human CD41A-PE, and anti-human CD34-PE-Cy7 (BD Biosciences). For functional experiments, we utilized anti-human vWF (Dako, 1:500) conjugated with anti-rabbit-AlexaFluor 647 (Biolegend). Then, cells were incubated for 30 min at room temperature, washed with PBS, centrifuged, resuspended in FACS buffer (PBS supplemented with 5% FBS and EDTA 2 mM) and stained with 7AAD cell viability solution (BD Biosciences).

To conduct platelet experiments, blood samples were collected into EDTA K2 Vacutainer tubes (BD Biosciences). Platelet-rich plasma (PRP) or supernatants from *in vitro* cell cultures were separated by centrifugation ($120 \times g$, 10 min), and a second centrifugation was required to obtain platelet pellets ($300 \times g$, 10 min). The platelets were resuspended in PBS-EDTA 2 mM and adjusted to a concentration of 1.5×10^5 platelets per tube. Antibody cocktails were added to each tube as previously described, and the samples were washed, centrifuged at $300 \times g$, and resuspended in 100 μL PBS-EDTA 2 mM.

After labeling, the cells and platelets were analyzed using either FACS Canto II or FACS Verse flow cytometers (BD Biosciences). Subsequently, the data were analyzed using Cytobank[69] software and visualized with GraphPad Prism (version 9.4.1).

BSS model generation: CRISPR-Cas9

The plasmid pSpCas9(BB)-2A-GFP (PX458) (Addgene plasmid #48138) was selected as the gene editing tool. Briefly, different sgRNAs were designed for each human single gene (*GP9*, *GP1BA*, and *GP1BB*) using BreakingCas[70] software. Their sequences are available in Table S4. sgRNAs were cloned into the plasmid following Feng Zhang's laboratory indications.[71] After cloning, plasmids were verified by Sanger sequencing and amplified by maxiprep (Macherey-Nagel).

For gene editing of megakaryoblastic cell lines, each construction was transfected into DAMI and MEG-01 using LipoD293T (Sinagen) as the delivery method; 1.2×10^6 cells resuspended in 1 mL RPMI 1640 were seeded in each well (six-well plate). Transfections were performed using 1.5 μg DNA and 6 μL LipoD per reaction, following the manufacturer's instructions. Forty-eight hours post-transfection, $EGFP^+$ cells were sorted using FACS Aria Fusion (BD Biosciences), establishing small pools (300 cells) in 96-well plates. Once expanded, cells were analyzed by flow cytometry and the most enriched pools were used to establish single-cell clones. Expanded single-cell clones were screened for GPIb-V-IX expression by flow cytometry. Genomic DNA (gDNA) was isolated from these GPIb-V-IX-negative clones to characterize these edited *loci* by Sanger sequencing.

To generate iPSCs *GP9*-KO, iPSC#1 was seeded at 30% confluence in T25 flasks. At 70%–80% confluence, iPSC cells were detached using 0.75X TrypLE Express, washed in PBS and centrifuged ($150 \times g$ for 5 min). The cell pellet was resuspended in E8 and 1.2×10^6 cells were nucleofected with 1.5 μg plasmid DNA (Nucleofector 2B, Lonza) using a Human Stem Cell Nucleofector Kit 1 (Lonza). After nucleofection, cells were seeded in Matrigel-coated six-well plates and cultured in E8 supplemented with 10 μM Y-27632. Forty-eight hours later, cells were individualized with TrypLE Express, sorted by $EGFP^+$ expression, and seeded in small pools (150 cells). gDNA was isolated from each pool, amplified by PCR, and sequenced by Sanger sequencing. KO enrichment frequency was analyzed by Synthego Performance Analysis, ICE Analysis. 2019. v3.0 (Synthego). Single-cell clones were isolated from the most enriched pools and screened by Sanger sequencing confirming *GP9 locus* edition.

Sanger sequencing

Plasmid DNA samples from *E. coli* DH5α or Stbl3 were processed with NucleoSpin Plasmid (Macherey-Nagel) and sequenced by StabVida laboratories.

High-throughput clone screening was performed using QuickExtract (Lucigen). Half of the 96-well was resuspended in lysis buffer, heated to 65°C for 6 min, vortexed, and heated to 98°C for 2 min. High-quality gDNA was obtained from established cell cultures using NucleoSpin Tissue (Macherey-Nagel) following manufacturer's indications.

PCR amplification of the mutated *loci* was completed with GoTaq G2 Flexi DNA Polymerase (Promega) following experimental conditions indicated in Table S5. Amplicons were purified using NucleoSpin Gel and PCR Clean-up (Macherey-Nagel) and sequenced in StabVida laboratories. The sequencing primers used are listed in Table S6, while the gene-edited alleles are described in Tables S1–S3.

ImageStream analysis

Cells and platelets were collected and stained as previously described in the flow cytometry analysis section. Stained cells were fixed with 4% paraformaldehyde (Merck Life Sciences) in PBS for 12 min and permeabilized with 0.1%Triton X-100 detergent (Thermo Scientific) in PBS for 20 min. Then, cells were incubated with 1 μM Hoechst (Merck Life Sciences) for 3 min, washed, and resuspended in FACS buffer. Similarly, platelets were stained, washed, and resuspended in PBS-EDTA 2 mM. Last, data were acquired in an ImageStream Mark II imaging flow cytometer (Amnis) and analyzed with IDEAS software (Amnis).

To determine platelet size, we used IDEAS software following these steps. First, we identified the $CD41^+$ platelet population (R1). Second, we applied a circularity filter (R2) and an additional filter to select focused images (R3). Next, we identified individual events and created a mask that covered the entire surface of the $CD41^+$ fluorescence signal from each platelet. Using all these masks, the IDEAS software calculated the mean diameter ± standard deviation (SD) of the selected populations.

Lentiviral vector constructs

SEIs2Rev is our reporter empty vector (R-EV). It is a self-inactivated LV that expresses the EGFP under the spleen focus-forming virus (SFFV) promoter. Additionally, it includes an insulator formed by a chimeric sequence composed of SAR2 and HS4-650 elements (IS2 insulator).[30] To produce our reporter vector-GPIX (R-GPIX), we used SEIs2Rev LV as a starting point and introduced a cassette containing the human megakaryocytic promoter (h*GP6L*) combined with the human WT *GP9* coding sequence (*hGP9*). Both sequences were obtained from NCBI and used to design specific primer pairs using different softwares (Primer3Plus and Primer-BLAST). Chosen primer pairs were modified to include a *PvuI* cutting site between promoter and CDS to facilitate the ligation process between both sequences. Next step was to amplify by PCR using gDNA from DAMI cells as a template. PCR conditions and primer sequences can be found in Table S2. PCR products were purified, digested with *PvuI,* and ligated with T4-ligase (New England Biolabs). The ligation product was PCR amplified using hGP6-FW and hGP9-RV, purified, and cloned into pCR2.1 (Invitrogen, Life Technologies). The therapeutic cassette cloned into this intermediate vector was flanked now by multicloning sites. *EcoRI* (New England Biolabs) was used to remove the *hGP6*-hGP9 sequence from the intermediate vector and to clone it in both orientations into SEIs2Rev empty vector. Optimal orientations for GPIX are shown in Figure 2A and were determined by EGFP and GPIX expression in DAMI *GP9*-KO transduced cells (data not shown).

Furthermore, to build our therapeutic empty vector (T-EV), we removed the SFFV-EGFP cassette from SEIs2Rev (R-EV). Similarly, starting from the R-GPIX LV, we built our therapeutic vector (T-GPIX).

Final constructs were sequenced as previously described. DNA constructs were transformed into *E. coli Stbl3* and maxiprep was performed to get high concentrated plasmids and sequenced in StabVida laboratories.

LVs production

LVs were produced by 293T cell co-transfection of (1) plasmid vector (R-EV, R-GPIX, T-EV, or T-GPIX), (2) pCMVDR8.91 packaging plasmid, and (3) VSV-G (pMD2.G) plasmids. 293T cells were transfected using LipoD293T as previously described in Benabdellah et al.[72] Supernatants were harvested at 48 h post-transfection by ultracentrifugation (SORVALL, WX ultra series centrifuge, Thermo Scientific) resuspending the viral pellet in non-supplemented RPMI. Viral titers were determined by performing serial dilutions of the concentrated LVs over DAMI *GP9*-KO cells. GPIX-positive cells were determined by flow cytometry 3–7 days after transduction. Vector titration was calculated according to the following formula:

$$Titer = \frac{10^5\ plated\ cells * \%GPIX\ cells/100}{mL\ vector}$$

Cell transduction

DAMI and MEG-01 cells were transduced with an MOI = 20, while iPSCs and HSC-BSS were transduced with MOI = 50. Required volume of LVs was added to culture media supplemented with 1 μg/mL protamine sulfate (Merck Life Sciences). iPSCs were exposed to two sequential transduction hits. Transduction was performed overnight, replacing culture media the following morning.

Functional assay: Ristocetin- GPIba-vWF binding

MEG-01 and transduced MEG-01 cells were used. For flow cytometry analysis, cells were incubated under four different conditions at 37°C for 30 min: Ristocetin (1 mg/mL, ABP) plus vWF (Haematologic Technologies) (10 μg/mL); only vWF, only ristocetin, and nothing. Following incubation, cells were stained as described in the flow cytometry analysis section.

To perform the sedimentation experiments, 5×10^6 cells/mL were resuspended in 250 μL PBS supplemented with 10 μg/mL vWF and ristocetin (1 mg/mL). After pre-incubating the samples at 37°C for 2 min under stirring conditions, we measured light transmission in a light-transmission aggregometer (Chrono-log) at 37°C for 15 min. Measurements were made by pairs: WT vs. *GP9*-KO, R-EV vs. R-GPIX, T-EV vs. T-GPIX. Additionally, we demonstrated the agglutination effect by photographing MEG-01 WT and *GP9*-KO cells incubated in suspension with vWF-ristocetin treatment after the pre-incubation period.

Functional assay: Botrocetin-GPIba mediated adhesion to vWF

Cell concentration was adjusted to a final concentration of 350,000 cells/mL and 100 μL was seeded over 96-well plates precoated with vWF (10 μg/mL) in PBS at 4°C overnight. For each cell line, we established four conditions: botrocetin (0.1 μg/mL), PBS-EDTA (10 mM), botrocetin+PBS-EDTA, and botrocetin+PBS-EDTA+6B4[73] antibody preincubated cells (10 μg/mL 6B4 for 30 min) for 90 min at 37°C. Then, the cells were washed three times with PBS, fixed, permeabilized, and stained with 1 μg/mL DAPI (4′,6-diamidino-2-phenylindole, ThermoFisher Scientific) and 2 μg/mL Phalloidin-tetramethylrhodamine B isothiocyanate (TRITC, Santa Cruz Animal Health) for 30 min at room temperature. Immunofluorescence pictures were made using an Axio Observer Z1 inverted fluorescence microscope (Zeiss). Cell number was determined using Fiji free software.[74]

iPSC differentiation toward megakaryocytic lineage

Megakaryocytic differentiation was performed using the Moreau et al. protocol.[25] Briefly, FLI1, TAL1, and GATA1 transcription factors were overexpressed from a commercially available LV (Flash Therapeutics). On day −1, 4, 5×10 iPSCs/well (12-well plate) were seeded in E8 medium supplemented with 10 μM Y-27632. On day 0, iPSC#1 were transduced with LV and cultured in E6 medium supplemented with FGF2 (20 ng/mL, Peprotech) and BMP4 (10 ng/mL, Peprotech). From day 2 to day 9, cells were grown in serum-free medium xeno-free (GMP SCGM, Cell Genix) supplemented with TPO (20 ng/mL, Peprotech) and SCF (25 ng/mL, Peprotech). Every 2 days, cell culture media was refreshed by half-media changes. On day 9, cells were detached with TrypLE Express, analyzed by flow cytometry, and split up to six-well plates. On day 15 and day 21, cells were analyzed again by flow cytometry. On day 35, the cells were centrifuged at $300 \times g$ for 5 min and resuspended in RPMI 1640 without FBS. Next day, the entire supernatant was collected and centrifuged twice to isolate the platelets. These were stained for flow cytometry analysis, as previously described.

HSC isolation and differentiation to megakaryocytic lineage

The study was approved by the Human Research Ethics Committee of the University of Granada. Patients signed the informed consent before sample extraction. Fifty milliliters of fresh blood from each BSS patient was collected in EDTA tubes. PRP from BSS patients was separated by gravity-mediated decantation for 40 min. PBMCs were isolated by centrifugation using Ficoll Paque PLUS (GE Healthcare) ($400 \times g$, 40 min, Accel 0, Brake 0). PBMCs were washed twice with PBS. The cell pellet was resuspended in 150 μL MACS Buffer and incubated with 50 μL anti-FCR and 50 μL anti-CD34 magnetic beads at 4°C for 30 min (CD34MicroBead Kit UltraPure, Miltenyi Biotech). After a washing step, we performed an immunomagnetic selection of $CD34^+$ cells with MS columns (Miltenyi Biotech). Negative fraction was used to isolate genomic DNA for *GP9 locus* PCR amplification and BSS patients' characterization by Sanger sequencing.

To differentiate HSCs to MKs, cells were grown in StemSpam (StemCell Technologies) combined with different cocktails regarding to the differentiation stage. On day 0, the positive fraction was expanded in StemSpam 1X PS supplemented with cytokine cocktail 1: SCF (100 ng/mL) + FLT3L (100 ng/mL, Peprotech) + TPO (100 ng/mL) + SR1 (0.75 μm = 322.12 ng/mL, StemCell Technologies) + UM171 (35 nM = 15.87 ng/mL, StemCell Technologies) + IL-6 (100 ng/mL, Peprotech). On day 2, expanded HSCs were transduced with R-GPIX and cultured with cytokine cocktail 2 (StemSpam + TPO [100 ng/mL] + FTL3 [100 ng/mL] + SCF [100 ng/mL] + 1% P/S). Day 3 begins differentiation phase I, where we are following megakaryoblast progenitor appearance (Cytokine cocktail 3: TPO 100 ng/mL + SCF 100 ng/mL + IL-6 7.5 ng/mL). Finally, megakaryocytic maturation is achieved in differentiation phase II, where TPO 100 ng/mL is the unique supplementary cytokine administrated.

Statistical analysis

Data were presented as mean ± standard deviation (SD). For comparison of >2 groups, we used ANOVA two-way plus Tukey multiple comparison test. Analyses over time were performed with two-way ANOVA and Holm-Šídák's multiple comparisons test. When one group was compared, we used ANOVA one-way or two-way with Dunnett's multiple comparisons test or Šídák's multiple comparisons test depending on the type of comparison performed. All these analyses were completed using GraphPad Prism (9.4.1).

DATA AVAILABILITY

The authors confirm that all data supporting the results included in this manuscript are available in the article document or in its accompanying supplemental materials.

SUPPLEMENTAL INFORMATION

Supplemental information can be found online at https://doi.org/10.1016/j.omtn.2023.06.008.

ACKNOWLEDGMENTS

The authors would like to thank all the students and researchers who have participated in the Bernard-Soulier syndrome research line initiated in 2015; especially to Dr. Lopez-Onieva, Dr. Lamolda, Ms. Beatriz Fernandez, Ms. Ana Marquez, Mr. Adrian Blanco, and Ms. Maria Martínez. Their research all over those years has served as the basis for this manuscript. In addition, to all the members of the Gene Regulation, Stem Cells and Development lab at GENyO. In addition, we thank Prof. Francoise Lanza (Université de Strasbourg, INSERM, Strasbourg, France) for providing anti-GPIbβ antibody. This study

was supported by FEDER/Junta de Andalucia-Consejeria de Transformacion Economica, Industria, Conocimiento y Universidades (B-CTS-676-UGR) to P.J.R.; the Spanish Health Institute Carlos III to P.J.R. (PI16/01340) and to F.M.: Red TerAv (RD21/0017/0001) (ISCIII–NextGenerationEU funds–Recovery and Resilience Mechanism) cofounded by the European Regional Development Fund "A way to build Europe," and the Ramon y Cajal (RYC-2015-18382) and PID2019-110153RB-I00 to P.J.R. founded by the Ministry of Economy and Competitiveness, and University of Granada for precompetitive research projects (No. 108) to G.M.-N. G.M.-N. is a PFIS fellow from the Spanish Health Institute Carlos III (FI17/00178) and received an EMBO scientific program grant (9618) for international mobility. J.C.-H. was supported by PhD program from the Ministry of Universities (FPU18/03410). I.S. was supported by the Young Researcher program from University of Granada and a donation from Rolucan Association (Rota Lucha Contra el Cancer). G.M.-N., J.C.-H., and I.S. were PhD students from the Doctoral Program in Biomedicine from University of Granada. P.L. was a fellow from the Research Initiation Scholarship Program from University of Granada.

AUTHOR CONTRIBUTIONS

G.M.-N.: designed and performed the investigation, developed methodology, data curation, formal analysis, analyzed the data, data and figure visualization, and wrote the original draft; J.C.-H., I.S., P.L., and S.D.-M.: performed the investigation; SPR data curation and Graduate and Master students supervision; U.M., J.A.G., and F.M.: provided resources and materials; T.S. and M.L.L. provided BSS patient samples; J.R.: developed methodology, provided BSS patient samples and data curation; V.R.: data curation and provided resources and materials; C.T.: developed methodology, data curation, and formal analysis and wrote the original draft; P.J.R.: conceptualization, funding acquisition, project administration, and research supervision, data and figure visualization, and wrote the original draft. All the authors reviewed the manuscript.

DECLARATION OF INTERESTS

The authors declare no competing interests.

REFERENCES

1. Berndt, M.C., and Andrews, R.K. (2011). Bernard-Soulier syndrome. Haematologica *96*, 355–359. https://doi.org/10.3324/haematol.2010.039883.

2. Andrews, R.K., and Berndt, M.C. (2013). Bernard-Soulier syndrome: an update. Semin. Thromb. Hemost. *39*, 656–662. https://doi.org/10.1055/s-0033-1353390.

3. Savoia, A., Pastore, A., De Rocco, D., Civaschi, E., Di Stazio, M., Bottega, R., Melazzini, F., Bozzi, V., Pecci, A., Magrin, S., et al. (2011). Clinical and genetic aspects of Bernard-Soulier syndrome: searching for genotype/phenotype correlations. Haematologica *96*, 417–423. https://doi.org/10.3324/haematol.2010.032631.

4. Li, R., and Emsley, J. (2013). The organizing principle of the platelet glycoprotein Ib-IX-V complex. J. Thromb. Haemostasis *11*, 605–614. https://doi.org/10.1111/jth.12144.

5. Savoia, A., Kunishima, S., de Rocco, D., Zieger, B., Rand, M.L., Pujol-Moix, N., Caliskan, U., Tokgoz, H., Pecci, A., Noris, P., et al. (2014). Spectrum of the Mutations in Bernard-Soulier Syndrome. Hum. Mutat. *35*, 1033–1045. https://doi.org/10.1002/humu.22607.

6. Boeckelmann, D., Hengartner, H., Greinacher, A., Nowak-Göttl, U., Sachs, U.J., Peter, K., Sandrock-Lang, K., and Zieger, B. (2017). Patients with Bernard-Soulier syndrome and different severity of the bleeding phenotype. Blood Cells Mol. Dis. *67*, 69–74. https://doi.org/10.1016/j.bcmd.2017.01.010.

7. Nurden, A.T., and Caen, J.P. (1975). Specific roles for platelet surface glycoproteins in platelet function. Nature *255*, 720–722.

8. Alamelu, J., and Liesner, R. (2010). Modern management of severe platelet function disorders. Br. J. Haematol. *149*, 813–823. https://doi.org/10.1111/j.1365-2141.2010.08191.x.

9. Seligsohn, U. (2012). Treatment of inherited platelet disorders. Haemophilia *18* (*Suppl 4*), 161–165. https://doi.org/10.1111/j.1365-2516.2012.02842.x.

10. Locatelli, F., Rossi, G., and Balduini, C. (2003). Hematopoietic stem-cell transplantation for the Bernard-Soulier syndrome. Ann. Intern. Med. *138*, 79.

11. Rieger, C., Rank, A., Fiegl, M., Tischer, J., Schiel, X., Ostermann, H., and Kolb, H.-J. (2006). Allogeneic stem cell transplantation as a new treatment option for patients with severe Bernard-Soulier Syndrome. Thromb. Haemostasis *95*, 190–191.

12. Wilcox, D.A. (2019). Gene Therapy for Platelet Disorders. In Platelets (Elsevier), pp. 1191–1205. https://doi.org/10.1016/B978-0-12-813456-6.00067-9.

13. Rogers, S. (1971). Gene therapy: a potentially invaluable aid to medicine and mankind. Res. Commun. Chem. Pathol. Pharmacol. *2*, 587–600.

14. Mamcarz, E., Zhou, S., Lockey, T., Abdelsamed, H., Cross, S.J., Kang, G., Ma, Z., Condori, J., Dowdy, J., Triplett, B., et al. (2019). Lentiviral Gene Therapy Combined with Low-Dose Busulfan in Infants with SCID-X1. N. Engl. J. Med. *380*, 1525–1534. https://doi.org/10.1056/nejmoa1815408.

15. Aiuti, A., Biasco, L., Scaramuzza, S., Ferrua, F., Cicalese, M.P., Baricordi, C., Dionisio, F., Calabria, A., Giannelli, S., Castiello, M.C., et al. (2013). Lentiviral hematopoietic stem cell gene therapy in patients with wiskott-aldrich syndrome. Science *341*, 1233151. https://doi.org/10.1126/science.1233151.

16. Ferrua, F., Cicalese, M.P., Galimberti, S., Giannelli, S., Dionisio, F., Barzaghi, F., Migliavacca, M., Bernardo, M.E., Calbi, V., Assanelli, A.A., et al. (2019). Lentiviral haemopoietic stem/progenitor cell gene therapy for treatment of Wiskott-Aldrich syndrome: interim results of a non-randomised, open-label, phase 1/2 clinical study. Lancet. Haematol. *6*, e239–e253. https://doi.org/10.1016/S2352-3026(19)30021-3.

17. Biffi, A., Montini, E., Lorioli, L., Cesani, M., Fumagalli, F., Plati, T., Baldoli, C., Martino, S., Calabria, A., Canale, S., et al. (2013). Lentiviral hematopoietic stem cell gene therapy benefits metachromatic leukodystrophy. Science *341*, 1233158. https://doi.org/10.1126/science.1233158.

18. Thompson, A.A., Walters, M.C., Kwiatkowski, J., Rasko, J.E.J., Ribeil, J.-A., Hongeng, S., Magrin, E., Schiller, G.J., Payen, E., Semeraro, M., et al. (2018). Gene Therapy in Patients with Transfusion-Dependent β-Thalassemia. N. Engl. J. Med. *378*, 1479–1493. https://doi.org/10.1056/nejmoa1705342.

19. Río, P., Navarro, S., Wang, W., Sánchez-Domínguez, R., Pujol, R.M., Segovia, J.C., Bogliolo, M., Merino, E., Wu, N., Salgado, R., et al. (2019). Successful engraftment of gene-corrected hematopoietic stem cells in non-conditioned patients with Fanconi anemia. Nat. Med. *25*, 1396–1401. https://doi.org/10.1038/s41591-019-0550-z.

20. Ware, J., Russell, S., and Ruggeri, Z.M. (2000). Generation and rescue of a murine model of platelet dysfunction: the Bernard-Soulier syndrome. Proc. Natl. Acad. Sci. USA *97*, 2803–2808. https://doi.org/10.1073/pnas.050582097.

21. Kanaji, S., Kuether, E.L., Fahs, S.A., Schroeder, J.A., Ware, J., Montgomery, R.R., and Shi, Q. (2012). Correction of murine Bernard-Soulier syndrome by lentivirus-mediated gene therapy. Mol. Ther. *20*, 625–632. https://doi.org/10.1038/mt.2011.231.

22. Strassel, C., Bull, A., Moog, S., Receveur, N., Mallo, L., Mangin, P., Eckly, A., Freund, M., Dubart-Kupperschmitt, A., Gachet, C., and Lanza, F. (2016). Lentiviral gene rescue of a Bernard-Soulier mouse model to study platelet glycoprotein Ibβ function. J. Thromb. Haemostasis *14*, 1470–1479. https://doi.org/10.1111/jth.13355.

23. Lu, S.-J., Li, F., Yin, H., Feng, Q., Kimbrel, E.A., Hahm, E., Thon, J.N., Wang, W., Italiano, J.E., Cho, J., and Lanza, R. (2011). Platelets generated from human embryonic stem cells are functional in vitro and in the microcirculation of living mice. Cell Res. *21*, 530–545. https://doi.org/10.1038/cr.2011.8.

24. Toscano, M.G., Navarro-Montero, O., Ayllon, V., Ramos-Mejia, V., Guerrero-Carreno, X., Bueno, C., Romero, T., Lamolda, M., Cobo, M., Martin, F., et al.

(2015). SCL/TAL1-mediated Transcriptional Network Enhances Megakaryocytic Specification of Human Embryonic Stem Cells. Mol. Ther. *23*, 158–170. https://doi.org/10.1038/mt.2014.196.

25. Moreau, T., Evans, A.L., Vasquez, L., Tijssen, M.R., Yan, Y., Trotter, M.W., Howard, D., Colzani, M., Arumugam, M., Wu, W.H., et al. (2016). Large-scale production of megakaryocytes from human pluripotent stem cells by chemically defined forward programming. Nat. Commun. *7*, 11208. https://doi.org/10.1038/ncomms11208.

26. Mekchay, P., Ingrungruanglert, P., Suphapeetiporn, K., Sosothikul, D., Ji-au, W., Maneesri Le Grand, S., Israsena, N., and Rojnuckarin, P. (2019). Study of Bernard–Soulier Syndrome Megakaryocytes and Platelets Using Patient-Derived Induced Pluripotent Stem Cells. Thromb. Haemostasis *119*, 1461–1470. https://doi.org/10.1055/s-0039-1693409.

27. Luo, S.-Z., Mo, X., Afshar-Kharghan, V., Srinivasan, S., López, J.A., and Li, R. (2007). Glycoprotein Ibα forms disulfide bonds with 2 glycoprotein Ibβ subunits in the resting platelet. Blood *109*, 603–609. https://doi.org/10.1182/blood-2006-05-024091.

28. Milone, M.C., and O'Doherty, U. (2018). Clinical use of lentiviral vectors. Leukemia *32*, 1529–1541. https://doi.org/10.1038/s41375-018-0106-0.

29. Latorre-Rey, L.J., Wintterle, S., Dütting, S., Kohlscheen, S., Abel, T., Schenk, F., Wingert, S., Rieger, M.A., Nieswandt, B., Heinz, N., and Modlich, U. (2017). Targeting expression to megakaryocytes and platelets by lineage-specific lentiviral vectors. J. Thromb. Haemostasis *15*, 341–355. https://doi.org/10.1111/jth.13582.

30. Benabdellah, K., Gutierrez-Guerrero, A., Cobo, M., Muñoz, P., and Martín, F. (2014). A chimeric HS4-SAR insulator (IS2) that prevents silencing and enhances expression of lentiviral vectors in pluripotent stem cells. PLoS One *9*, e84268. https://doi.org/10.1371/journal.pone.0084268.

31. Cruz, M.A., Handin, R.I., and Wise, R.J. (1993). The interaction of the von Willebrand factor-A1 domain with platelet glycoprotein Ib/IX. The role of glycosylation and disulfide bonding in a monomeric recombinant A1 domain protein. J. Biol. Chem. *268*, 21238–21245.

32. Coller, B.S. (1978). The effects of ristocetin and von Willebrand factor on platelet electrophoretic mobility. J. Clin. Invest. *61*, 1168–1175. https://doi.org/10.1172/JCI109032.

33. Dong, J.-F., Berndt, M.C., Schade, A., McIntire, L.V., Andrews, R.K., and López, J.A. (2001). Ristocetin-dependent, but not botrocetin-dependent, binding of von Willebrand factor to the platelet glycoprotein Ib-IX-V complex correlates with shear-dependent interactions.

34. Wu, D., Meiring, M., Kotze, H.F., Deckmyn, H., and Cauwenberghs, N. (2002). Inhibition of Platelet Glycoprotein Ib, Glycoprotein IIb/IIIa, or Both by Monoclonal Antibodies Prevents Arterial Thrombosis in Baboons. Arterioscler. Thromb. Vasc. Biol. *22*, 323–328. https://doi.org/10.1161/hq0202.102321.

35. Palma-Barqueros, V., Revilla, N., Sánchez, A., Zamora Cánovas, A., Rodriguez-Alén, A., Marín-Quílez, A., González-Porras, J.R., Vicente, V., Lozano, M.L., Bastida, J.M., and Rivera, J. (2021). Inherited Platelet Disorders: An Updated Overview. Int. J. Mol. Sci. *22*, 4521. https://doi.org/10.3390/ijms22094521.

36. Noris, P., Simsek, S., Stibbe, J., and von dem Borne, A.E. (1997). A phenylalanine-55 to serine amino-acid substitution in the human glycoprotein IX leucine-rich repeat is associated with Bernard-Soulier syndrome. Br. J. Haematol. *97*, 312–320. https://doi.org/10.1046/j.1365-2141.1997.582706.x.

37. Dong, J.F., Gao, S., and López, J.A. (1998). Synthesis, assembly, and intracellular transport of the platelet glycoprotein Ib-IX-V complex. J. Biol. Chem. *273*, 31449–31454. https://doi.org/10.1074/jbc.273.47.31449.

38. Fischer, S., Handrick, R., and Otte, K. (2015). The art of CHO cell engineering: A comprehensive retrospect and future perspectives. Biotechnol. Adv. *33*, 1878–1896. https://doi.org/10.1016/j.biotechadv.2015.10.015.

39. Suzuki, K., Hayashi, T., Akiba, J., Satoh, S., and Kato, T. (1999). Phenotypic Consequence of the Gene Abnormality in the Platelet Glycoprotein IX Gene Observed in a Patient with Bernard-Soulier Syndrome through Mammalian Cell Expression System. Thromb. Res. *95*, 295–302. https://doi.org/10.1016/S0049-3848(99)00047-X.

40. Lanza, F., De La Salle, C., Baas, M.-J., Schwartz, A., Boval, B., Cazenave, J.-P., and Caen, J.P. (2002). A Leu7Pro mutation in the signal peptide of platelet glycoprotein (GP)IX in a case of Bernard-Soulier syndrome abolishes surface expression of the GPIb-V-IX complex. Br. J. Haematol. *118*, 260–266. https://doi.org/10.1046/j.1365-2141.2002.03544.x.

41. Wang, Z., Zhao, X., Duan, W., Fu, J., Lu, M., Wang, G., Bai, X., and Ruan, C. (2004). A novel mutation in the transmembrane region of glycoprotein IX associated with Bernard-Soulier syndrome. Thromb. Haemostasis *92*, 606–613. https://doi.org/10.1160/TH04-04-0240.

42. STRASSEL, C., DAVID, T., ECKLY, A., Baas, M.J., MOOG, S., RAVANAT, C., Trzeciak, M.C., VINCIGUERRA, C., Cazenave, J.P., GACHET, C., and Lanza, F. (2006). Synthesis of GPIbβ with novel transmembrane and cytoplasmic sequences in a Bernard–Soulier patient resulting in GPIb-defective signaling in CHO cells. J. Thromb. Haemostasis *4*, 217–228. https://doi.org/10.1111/j.1538-7836.2005.01654.x.

43. Moran, N., Morateck, P.A., Deering, A., Ryan, M., Montgomery, R.R., Fitzgerald, D.J., and Kenny, D. (2000). Surface expression of glycoprotein Ibα is dependent on glycoprotein Ibβ: evidence from a novel mutation causing Bernard-Soulier syndrome. Blood *96*, 532–539. https://doi.org/10.1182/blood.V96.2.532.

44. Strassel, C., Pasquet, J.-M., Alessi, M.-C., Juhan-Vague, I., Chambost, H., Combrié, R., Nurden, P., Bas, M.-J., De La Salle, C., Cazenave, J.-P., et al. (2003). A Novel Missense Mutation Shows that GPIbβ Has a Dual Role in Controlling the Processing and Stability of the Platelet GPIb-IX Adhesion Receptor. Biochemistry *42*, 4452–4462. https://doi.org/10.1021/bi026213d.

45. Takata, Y., Kanaji, T., Moroi, M., Seki, R., Sano, M., Nakazato, S., Sueoka, E., Imamura, Y., and Okamura, T. (2012). Platelets with a W127X mutation in GPIX express sufficient residual amounts of GPIbα to support adhesion to von Willebrand factor and collagen. Int. J. Hematol. *96*, 733–742. https://doi.org/10.1007/s12185-012-1216-5.

46. Sumitha, E., Jayandharan, G.R., David, S., Jacob, R.R., sankari devi, G., Bargavi, B., Shenbagapriya, S., Nair, S.C., Abraham, A., George, B., et al. (2011). Molecular basis of Bernard–Soulier syndrome in 27 patients from India. J. Thromb. Haemostasis *9*, 1590–1598. https://doi.org/10.1111/j.1538-7836.2011.04417.x.

47. Ali, S., Ghosh, K., and Shetty, S. (2014). Novel genetic abnormalities in Bernard-Soulier syndrome in India. Ann. Hematol. *93*, 381–384. https://doi.org/10.1007/s00277-013-1895-x.

48. Ghalloussi, D., Rousset-Rouvière, C., Popovici, C., Garaix, F., Saut, N., Saultier, P., Tsimaratos, M., Chambost, H., Alessi, M.C., and Baccini, V. (2020). Bernard–Soulier syndrome: first human case due to a homozygous deletion of GP9 gene. Br. J. Haematol. *188*, e87–e90. https://doi.org/10.1111/bjh.16374.

49. Noda, M., Fujimura, K., Takafuta, T., Shimomura, T., Fujimoto, T., Yamamoto, N., Tanoue, K., Arai, M., Suehiro, A., Kakishita, E., et al. (1995). Heterogenous Expression of Glycoprotein Ib, IX and V in Platelets from Two Patients with Bernard-Soulier Syndrome Caused by Different Genetic Abnormalities. Thromb. Haemostasis *74*, 1411–1415. https://doi.org/10.1055/s-0038-1649956.

50. Kunishima, S., Yamada, T., Hamaguchi, M., and Saito, H. (2006). Bernard-Soulier Syndrome due to GPIX W127X Mutation in Japan Is Frequently Misdiagnosed as Idiopathic Thrombocytopenic Purpura. Int. J. Hematol. *83*, 366–367. https://doi.org/10.1532/IJH97.06017.

51. Hadjkacem, B., Elleuch, H., Gargouri, J., and Gargouri, A. (2009). Bernard-Soulier syndrome: Novel nonsense mutation in GPIbβ gene affecting GPIb-IX complex expression. Ann. Hematol. *88*, 465–472. https://doi.org/10.1007/s00277-008-0611-8.

52. Strassel, C., Pasquet, J.M., Alessi, M.C., Juhan-Vague, I., Chambost, H., Combrié, R., Nurden, P., Bas, M.J., De La Salle, C., Cazenave, J.P., et al. (2003). A novel missense mutation shows that GPIbβ has a dual role in controlling the processing and stability of the platelet GPIb-IX adhesion receptor. Biochemistry *42*, 4452–4462. https://doi.org/10.1021/bi026213d.

53. Tang, J., Stern-Nezer, S., Liu, P.C., Matyakhina, L., Riordan, M., Luban, N.L.C., Steinbach, P.J., and Kaler, S.G. (2004). Mutation in the leucine-rich repeat C-flanking region of platelet glycoprotein Ib β impairs assembly of von Willebrand factor receptor. Thromb. Haemostasis *92*, 75–88. https://doi.org/10.1160/TH-04-02-0071.

54. Minkov, M., Zeitlhofer, P., Zoubek, A., Kager, L., Panzer, S., and Haas, O.A. (2020). Novel Compound Heterozygous Mutations in Two Families With Bernard–Soulier Syndrome. Front. Pediatr. *8*, 589812. https://doi.org/10.3389/fped.2020.589812.

55. Bragadottir, G., Birgisdottir, E.R., Gudmundsdottir, B.R., Hilmarsdottir, B., Vidarsson, B., Magnusson, M.K., Larsen, O.H., Sorensen, B., Ingerslev, J., and Onundarson, P.T. (2015). Clinical phenotype in heterozygote and biallelic Bernard-Soulier syndrome-A case control study. Am. J. Hematol. *90*, 149–155. https://doi.org/10.1002/ajh.23891.

56. Özdemir, Z.C., Düzenli Kar, Y., Ceylaner, S., and Bör, Ö. (2020). A novel mutation in the GP1BA gene in Bernard-Soulier syndrome. Blood Coagul. Fibrinolysis *31*, 83–86. https://doi.org/10.1097/MBC.0000000000000868.

57. McEwan, P.A., Yang, W., Carr, K.H., Mo, X., Zheng, X., Li, R., and Emsley, J. (2011). Quaternary organization of GPIb-IX complex and insights into Bernard-Soulier syndrome revealed by the structures of GPIβ and a GPIβ/GPIX chimera. Blood *118*, 5292–5301. https://doi.org/10.1182/blood-2011-05-356253.

58. Kato, K., Martinez, C., Russell, S., Nurden, P., Nurden, A., Fiering, S., and Ware, J. (2004). Genetic deletion of mouse platelet glycoprotein Ibbeta produces a Bernard-Soulier phenotype with increased alpha-granule size. Blood *104*, 2339–2344. https://doi.org/10.1182/blood-2004-03-1127.

59. Mohan, G., Malayala, S. v, Mehta, P., and Balla, M. (2020). A Comprehensive Review of Congenital Platelet Disorders. Cureus *12*, e11275. https://doi.org/10.7759/cureus.11275.

60. Mekchay, P., Ingrungruanglert, P., Suphapeetiporn, K., Sosothikul, D., Ji-Au, W., Maneesri Le Grand, S., Israsena, N., and Rojnuckarin, P. (2019). Study of bernard-soulier syndrome megakaryocytes and platelets using patient-derived induced pluripotent stem cells. Thromb. Haemostasis *119*, 1461–1470. https://doi.org/10.1055/s-0039-1693409.

61. Kovacevic, K.D., Grafeneder, J., Schörgenhofer, C., Gelbenegger, G., Gager, G., Firbas, C., Quehenberger, P., Jilma-Stohlawetz, P., Bileck, A., Zhu, S., et al. (2022). The von Willebrand factor A-1 domain binding aptamer BT200 elevates plasma levels of von Willebrand factor and factor VIII: a first-in-human trial. Haematologica *107*, 2121–2132. https://doi.org/10.3324/haematol.2021.279948.

62. Hrdinova, J., Fernández, D.I., Ercig, B., Tullemans, B.M.E., Suylen, D.P.L., Agten, S.M., Jurk, K., Hackeng, T.M., Vanhoorelbeke, K., Voorberg, J., et al. (2022). Structure-Based Cyclic Glycoprotein Ibα-Derived Peptides Interfering with von Willebrand Factor-Binding, Affecting Platelet Aggregation under Shear. Int. J. Mol. Sci. *23*, 2046. https://doi.org/10.3390/ijms23042046.

63. Vettore, S., Tezza, F., Malara, A., Vianello, F., Pecci, A., Scandellari, R., Floris, M., Balduini, A., and Fabris, F. (2011). A A386g biallelic GPIbα gene mutation with anomalous behavior: A new mechanism suggested for Bernard-Soulier syndrome pathogenesis. Haematologica *96*, 1878–1882. https://doi.org/10.3324/haematol.2010.039008.

64. Shimizu, Y., Kawashiri, S.Y., Nobusue, K., Nonaka, F., Tamai, M., Honda, Y., Yamanashi, H., Nakamichi, S., Kiyama, M., Hayashida, N., et al. (2022). Association between circulating CD34-positive cell count and height loss among older men. Sci. Rep. *12*, 7175. https://doi.org/10.1038/s41598-022-11040-y.

65. Iurlo, A., Galli, N., Bucelli, C., Artuso, S., Consonni, D., and Cattaneo, D. (2023). Trend of circulating CD34+ cells in patients with myelofibrosis: Association with spleen response during ruxolitinib treatment. Br. J. Haematol. *200*, 315–322. https://doi.org/10.1111/bjh.18526.

66. Mehta, A., Tahhan, A.S., Liu, C., Dhindsa, D.S., Nayak, A., Hooda, A., Moazzami, K., Islam, S.J., Rogers, S.C., Almuwaqqat, Z., et al. (2020). Circulating Progenitor Cells in Patients With Coronary Artery Disease and Renal Insufficiency. JACC. Basic Transl. Sci. *5*, 770–782. https://doi.org/10.1016/j.jacbts.2020.06.006.

67. Chen, G., Gulbranson, D.R., Hou, Z., Bolin, J.M., Ruotti, V., Probasco, M.D., Smuga-Otto, K., Howden, S.E., Diol, N.R., Propson, N.E., et al. (2011). Chemically defined conditions for human iPSC derivation and culture. Nat. Methods *8*, 424–429. https://doi.org/10.1038/nmeth.1593.

68. Perrault, C., Moog, S., Rubinstein, E., Santer, M., Baas, M.-J., de La Salle, C., Ravanat, C., Dambach, J., Freund, M., Santoso, S., et al. (2001). A Novel Monoclonal Antibody against the Extracellular Domain of GPIb Modulates vWF Mediated Platelet Adhesion.

69. Kotecha, N., Krutzik, P.O., and Irish, J.M. (2010). Web-based analysis and publication of flow cytometry experiments. Curr. Protoc. Cytom. *10*, 10.17. https://doi.org/10.1002/0471142956.cy1017s53.

70. Oliveros, J.C., Franch, M., Tabas-Madrid, D., San-León, D., Montoliu, L., Cubas, P., and Pazos, F. (2016). Breaking-Cas-interactive design of guide RNAs for CRISPR-Cas experiments for ENSEMBL genomes. Nucleic Acids Res. *44*, W267–W271. https://doi.org/10.1093/NAR/GKW407.

71. Ran, F.A., Hsu, P.D., Wright, J., Agarwala, V., Scott, D.A., and Zhang, F. (2013). Genome engineering using the CRISPR-Cas9 system. Nat. Protoc. *8*, 2281–2308. https://doi.org/10.1038/nprot.2013.143.

72. Benabdellah, K., Muñoz, P., Cobo, M., Gutierrez-Guerrero, A., Sánchez-Hernández, S., Garcia-Perez, A., Anderson, P., Carrillo-Gálvez, A.B., Toscano, M.G., and Martin, F. (2016). Lent-On-Plus Lentiviral vectors for conditional expression in human stem cells. Sci. Rep. *6*, 37289. https://doi.org/10.1038/srep37289.

73. Fontayne, A., Vanhoorelbeke, K., Pareyn, I., van Rompaey, I., Meiring, M., Lamprecht, S., Roodt, J., Desmet, J., and Deckmyn, H. (2006). Rational humanization of the powerful antithrombotic anti-GPIbα antibody: 6B4. Thromb. Haemostasis *96*, 671–684. https://doi.org/10.1160/TH06-06-0297.

74. Schindelin, J., Arganda-Carreras, I., Frise, E., Kaynig, V., Longair, M., Pietzsch, T., Preibisch, S., Rueden, C., Saalfeld, S., Schmid, B., et al. (2012). Fiji: An open-source platform for biological-image analysis. Nat. Methods *9*, 676–682. https://doi.org/10.1038/nmeth.2019.